Mechanisms for climate variability during glacial and interglacial periods

Jolene L. Loving
Department of Ocean Sciences, University of California, Santa Cruz, California, USA

Geoffrey K. Vallis
Geophysical Fluid Dynamics Laboratory, Princeton University, Princeton, New Jersey, USA

Received 7 November 2004; revised 31 May 2005; accepted 26 August 2005; published 17 December 2005.

[1] This paper suggests and explores mechanisms relevant to millennial-scale climate variability during glacial periods. In particular, we present the results of model studies that are able to reproduce many aspects of observed glacial climate variability (e.g., Dansgaard-Oeschger oscillations) without external forcing and that provide a natural explanation for the prevalence of high-amplitude variability in glacial climates and the relative stability of the Holocene. We show that the role of sea ice is critical to cold climate variability because of the effective reduction in the high-latitude meridional sea surface temperature gradient resulting from sea ice expansion and the associated role of sea ice in inhibiting heat flux from the ocean to atmosphere. Thus as sea ice expands in a cooler climate, the high-latitude oceanic heat loss to the atmosphere is inhibited, the thermohaline circulation weakens, and the sinking regions move equatorward, leading to a shallower and weaker deep circulation. This weak circulation is unstable, and intermittent high-amplitude oscillations occur on a timescale and with a spatial structure very similar to Dansgaard-Oeschger cycles. Consistent results are found using both a three-dimensional ocean circulation model coupled to an energy balance atmospheric model and with a much simpler ocean box model. In general, freshening plays a secondary role in the weakening of the North Atlantic thermohaline circulation. Significant freshening is required to alter the stable northern deepwater formation that occurs in a warm climate such as today's Holocene, but once this freshening threshold is achieved, the thermohaline circulation shifts to reverse overturning with sinking in the tropics.

Citation: Loving, J. L., and G. K. Vallis (2005), Mechanisms for climate variability during glacial and interglacial periods, *Paleoceanography*, *20*, PA4024, doi:10.1029/2004PA001113.

1. Introduction

[2] Several aspects of the geological record from the last glacial period have continued to lack adequate explanation. In particular, the high-amplitude variability in temperature on millennial timescales (Dansgaard-Oeschger cycles), as well as abrupt transitions between North Atlantic thermohaline circulation states remain perplexing [*Dansgaard et al.*, 1984, 1993; *Sarnthein et al.*, 1995; *Clark et al.*, 2002; *Pflaumann et al.*, 2003]. In this paper, we show how these and other features of glacial climates may arise naturally from the prevailing cold conditions.

[3] The geologic evidence for Dansgaard-Oeschger events is widespread over much of the Northern Hemisphere so the mechanisms involved must influence climate on a correspondingly large scale [*Keigwin et al.*, 1994; *Broecker and Hemming*, 2001; *Voelker*, 2002]. Since oceanic heat transport by the thermohaline circulation has potential for global impact, its variability would provide an explanation for glacial warm cycles [*Keigwin et al.*, 1994; *Ganachaud and Wunsch*, 2000; *Broecker and Hemming*, 2001]. However, although the variability and possible multiple equilibrium states of the thermohaline circulation have long been thought relevant to this issue [*Stommel*, 1961; *Manabe and Stouffer*, 1988], a robust mechanism for producing self-sustained oscillations, which are of a large magnitude only in a glacial climate, and require no external triggering, has remained elusive. Furthermore, the increased overall pole-to-equator atmosphere temperature gradient of glacial climates might suggest a more vigorous and perhaps more stable thermohaline circulation, whereas the opposite appears to have been the case [*CLIMAP Project Members*, 1976; *Broecker*, 1996; *Ruhlemann et al.*, 1999]. Nevertheless, proxies for low temperatures, and for reductions in North Atlantic Deep Water production, coincide in ocean sediments, suggesting that weaker North Atlantic Deep Water formation was associated with high-latitude cooling during glacial periods [*Boyle and Keigwin*, 1985; *Keigwin and Jones*, 1994; *Keigwin and Lehman*, 1994; *Rutberg et al.*, 2000]. This evidence supports the hypothesis that climate variability during the last glacial period is linked to reductions in northern heat transport by the thermohaline circulation.

[4] Most attempts to explain glacial cooling and variability have focused on steady or periodic high-latitude freshening of the North Atlantic [*Stocker and Wright*, 1991; *Weaver et al.*, 1991; *Manabe and Stouffer*, 1995, 1997;

0883-8305/05/2004PA001113$12.00

Sakai and Peltier, 1997, 1999; *Ganopolski and Rahmstorf*, 2001; *Clark et al.*, 2002; *Rahmstorf*, 2002]. Typically, applied freshwater forcing induces switching between states of thermohaline circulation and one explanation for glacial climate variability is periodic switches between circulation states [*Alley et al.*, 2001; *Rahmstorf*, 2003]. Here we show that cold conditions alone are sufficient to produce weakness in the thermohaline circulation, switches between circulation states and climate variability which are physically similar to Dansgaard-Oeschger cycles. With this "cold climate" mechanism, no external freshwater forcing is required to explain the observed variability in the North Atlantic region during the last glacial period.

[5] Although geologic evidence supports a link between climate variability during the last glacial period and reductions in northern heat transport by the thermohaline circulation, a direct connection between high-latitude freshening and thermohaline circulation variability is not always apparent. For example, there is an increase in the strength of the thermohaline circulation and rapid warming following large surface fluxes of fresh water (~0.16 Sv) during Heinrich events [*Heinrich*, 1988; *MacAyeal*, 1993]. So a mechanism, such as the one we present, for climate variability during cold periods which does not require external freshwater forcing is consistent with the geologic record for the North Atlantic region during the last glacial period.

[6] In order to separate the effects of cooling the climate system from the effects of high-latitude freshening we conduct two sets of experiments: First, we cool the atmosphere without changing the salinity forcing to simulate glacial cooling ("cooling without freshening"). Second, we increase high-latitude freshening without changing the surface temperature ("warm climate with freshening").

[7] Both of our experiment sets start with the same warm climate experiment (control experiment) that exhibits thermohaline circulation characteristics which are similar to the current North Atlantic thermohaline circulation. In our analysis we include a detailed comparison between our model results and the geologic record for the last glacial period.

[8] The organization of this paper is as follows. In section 2 we briefly describe our models. A more detailed description of the four-box model is in the Appendix. In section 3 we describe the results of experiments with our coupled three-dimensional ocean model and include a detailed comparison between our three-dimensional model results and the geologic record for the last glacial period. For analysis purposes we include similar experiments with a simple four-box ocean model (section 4). In section 5 we discuss our conclusions.

2. Models

[9] We use two types of coupled ocean models to perform our experiment sets. For the most realistic simulations, we use a single-hemisphere three-dimensional ocean model coupled to an energy balance atmosphere model and a thermodynamic sea ice model. A single-hemisphere model is appropriate for this study because, although there is some evidence for Dansgaard-Oeschger cycles in the Southern Hemisphere, they are most prevalent in the North Atlantic region (which suggests that they originate there). We certainly do not preclude interhemispheric effects in the Atlantic Ocean, but it behooves us to try to explain glacial variability in the simplest possible way, with the simplest possible geometry.

[10] For analysis of our three-dimensional results we use a simple four-box ocean model coupled to a very simple energy balance atmosphere model and include a sea ice parameterization. The results from this box model generally corroborate results from our three-dimensional model (and geologic evidence), and the box model is a tool for isolating physical mechanisms underlying our findings.

2.1. Three-Dimensional Ocean Model

[11] Our ocean model is a hydrostatic, Boussinesq, planetary geostrophic ocean model, with both temperature and salinity, in a rectangular ocean basin which extends from approximately 15°N to approximately 65°N and which is approximately 50° in zonal extent [*Samelson and Vallis*, 1996, 1997]. The horizontal resolution is about 1.5° and there are 32 depth layers. The surface boundary conditions include a fixed zonal wind profile, a baseline freshwater flux specified as evaporation minus precipitation (Figure 1) and sensible heat flux which is proportional to the difference between the sea surface temperature and the near-surface atmosphere temperature, as calculated by the energy balance atmosphere model. The freshwater flux associated with melting and freezing sea ice is added to the baseline freshwater flux (Figure 1).

2.2. Energy Balance Atmosphere Model

[12] Our energy balance atmosphere model is two-dimensional but otherwise of a standard type with a diffusive horizontal heat transport and radiation scheme which follows that of Fanning and Weaver [*Fanning and Weaver*, 1996].

[13] The atmosphere temperature evolution is calculated by

$$\rho H C_a \frac{dT_a}{dt} = S_0(1-\alpha) - e\sigma T_a^4 + \rho D H C_a \nabla^2 T_a + \rho C_H C_a U \cdot (T_0 - T_a) \quad (1)$$

[14] The temperature of the atmosphere is determined by the balance among insolation ($S_0(1-\alpha)$), outgoing infrared radiation ($e\sigma T_a^4$), sensible heat transfer between the atmosphere and ocean ($\rho C_H C_a U(T_o - T_a)$) and horizontal transport of heat in the form of diffusion ($\rho D H C_a \nabla^2 T_a$). Refer to Table 1 for energy balance and ice model constants. The surface albedo is increased by 0.20 when the ice thickness exceeds 0.2 m at any grid point. To incorporate random climate effects (weather) we include stochastic forcing on the atmosphere temperature.

[15] We use planetary emissivity (e) as a parameter to simulate colder or warmer climates. Ice core data show that the concentrations of greenhouse gases (methane and carbon dioxide) in the atmosphere were significantly lower during the last glacial maximum than they are today [*Jouzel et al.*, 1993]. Reducing greenhouse gases reduces the effective emitting height of the atmosphere and cools the

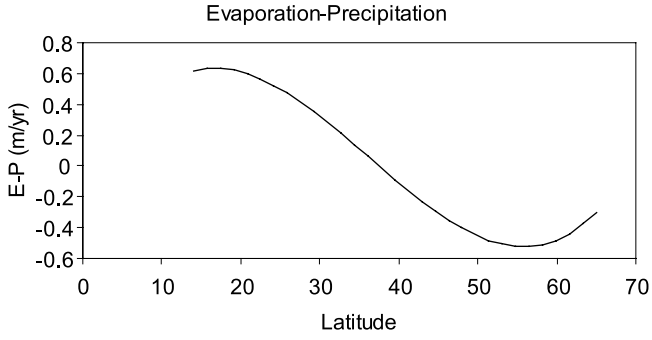

Figure 1. Baseline latitudinal evaporation minus precipitation (E−P) profile for the freshwater flux at the ocean surface. This baseline flux is used in the warm Holocene control experiments and in all experiments without applied surface freshening. For experiments where the magnitude of freshening is increased, this baseline function is multiplied by 1.3, 1.6, 2.0 and 4.0. Changes in surface freshwater forcing due to melting and freezing sea ice are added to this baseline profile.

climate, and in our model increasing the planetary emissivity (e) is a parameterization for this.

2.3. Thermodynamic Sea Ice Model

[16] Our sea ice model is based on *Semtner*'s [1976] zero layer ice model and *Parkinson and Washington*'s [1979] sea ice model.

[17] Ice is initially formed when the surface temperature of the ocean is below the freezing point (271.2 K). The thickness of the newly formed ice (H) is determined by the following equation:

$$H = \frac{(T_b - T_o)(d_{mix})(C_w)}{Q_1} \quad (2)$$

T_o is the sea surface temperature and H is the ice thickness. Refer to Table 1 for additional constants. When ice forms it is presumed to cover a complete grid point. Equation (2) is used as a test for a minimum ice thickness (0.2 m) which covers a complete grid point. Fluxes between the atmosphere and ocean are calculated as if there is no ice until this minimum is achieved. After ice is initially formed, the ocean surface temperature is set to the freezing point. Thus the newly formed ice releases the exact amount of energy required to keep the ocean surface layer at the freezing point.

[18] Once ice forms, ablation and accretion of ice at the bottom is determined by the following equation:

$$Q_1 \frac{dH}{dt} = \frac{k_1(T_b - T_s)}{H} + k_2(T_b - T_o) + Q_1\left(k_3 \nabla^2 H\right) \quad (3)$$

[19] The freshwater flux from melting or freezing ice is added to or subtracted from the baseline E-P curve (Figure 1), and 1 m of melted ice produces 0.96 m of freshwater flux into the ocean surface. Freshwater fluxes in the region of deep water formation are known to be an important factor in stability of the thermohaline circulation [*Broecker et al.*, 1990; *Fanning and Weaver*, 1996; *Manabe and Stouffer*, 1997; *Sakai and Peltier*, 1997]. Conduction through the ice ($k_1(T_b - T_s)/H$) and sensible heat transfer between the ocean and the ice ($k_2(T_b - T_o)$) are balanced at the bottom of the ice. The diffusion term ($k_3\nabla^2 H$) allows for horizontal transport of ice. When ice is present the temperature at the bottom of the ice (T_b) is set to the freezing point (271.2 K) and the temperature at the top of the ice (T_s) is set to the temperature of the atmosphere.

[20] When there is no growth at the top of the ice, the conductive flux through the ice ($k_1(T_b - T_s)/H$) must equal the heat flux (F_{ia}) from the surface of the ice into the atmosphere [*Lohmann and Gerdes*, 1998]. The flux balance at the top of the ice is

$$0 = \frac{k_1(T_b - T_s)}{H} + F_{ia} \quad (4)$$

[21] The conductive heat flux through the ice ($k_1(T_b - T_s)/H$) is calculated based on the difference between the temperature at the bottom of the ice (T_b, freezing point) and the temperature at the top surface of the ice (T_s). We assume that the temperature at the surface of the ice is equal to the atmosphere temperature ($T_s = T_a$). Since the conductive heat flux through the ice must exactly balance the heat flux from the ice to the atmosphere when there is no ice growth at the top surface (equilibrium), in our model the conductive heat flux ($k_1(T_b - T_a)/H$) is transferred directly to the atmosphere.

2.4. Four-Box Coupled Model

[22] Our four-box ocean model is based on Winton's three box halocline oscillator [*Winton*, 1993]. We added a midlatitude surface box (three surface boxes), vertical heat transport between the surface ocean boxes and a simple atmosphere. The midlatitude box is important, because reconstructions of glacial thermohaline circulation suggest that the sinking region for North Atlantic Deep Water formation may have shifted southward from the Nordic Seas to the North Atlantic [*Duplessy et al.*, 1988; *Bigg et al.*, 2000]. Our coupled atmosphere is based on *Rahmstorf*'s [1994] atmosphere model with a restoring term for the atmosphere temperature that parameterizes the effect of radiative heat transport.

Table 1. Constants for Ice Model and Energy-Balance-Atmosphere Model[a]

Symbol	Description	Value
T_b	temperature at bottom of ice	271.2
d_{mix}	depth of mixed layer	25 m
Q_1	heat of fusion of ice	302 MJ m^{-3}
C_w	volumetric heat capacity of water	4.19 MJ m^{-3} K^{-1}
k_1	thermal conductivity of ice	2.04 W m^{-1} K^{-1}
k_2	sensible heat between ocean and ice	200 W m^{-2} K^{-1}
k_3	horizontal "diffusion" of ice	0.001 m^2 s^{-1}
ρ	surface air density	1.25 kg m^{-3}
H	atmosphere scale height	8400 m
C_a	heat capacity of dry air	10^3 J kg^{-1} K^{-1}
σ	Stephan-Boltzman constant	5.67×10^{-8} W m^{-2} K^{-4}
C_H	Stanton number	1.75×10^{-3}
U	wind speed	5.0 m s^{-1}
D	atmospheric heat diffusion coefficient	1.23×10^6 m^2 s^{-1}

[a]Sources are *Semtner* [1976], *Parkinson and Washington* [1979], and *Fanning and Weaver* [1996].

[23] The box model includes a fractional sea ice cover (α) over the high-latitude and midlatitude surface boxes. The fractional ice cover (α) varies linearly with the atmosphere temperature of the high-latitude box. When the high-latitude atmosphere temperature is 271 K or above there is no ice ($\alpha = 0$), and when the high-latitude atmosphere temperature is 261 K or below, the high-latitude box is completely covered with ice ($\alpha = 1.0$). This ice cover does not include feedback from melting and freezing ice but does include ice-albedo feedback on temperature and a lower limit to the high-latitude ocean restoring temperature when sea ice is present. Ice-albedo feedback enhances high-latitude cooling and warming during Dansgaard-Oeschger events and sea ice acts as an insulator between the atmosphere and the ocean. When sea ice is present the ocean surface temperature forcing is effectively fixed at the freezing point, and this serves to flatten the high-latitude temperature forcing at the ocean surface. Small-amplitude changes in the thermohaline circulation may be amplified by "switch-like" changes in sea ice because the insulating effect of sea ice and ice-albedo feedback combine to enhance atmospheric temperature changes when sea ice melts and forms [*Kaspi et al.*, 2004; *Gildor and Tziperman*, 2003]. The equations for the four-box coupled model are given in the Appendix.

3. Three-Dimensional Coupled Model Experiments

[24] We conduct two sets of experiments with our coupled atmosphere/sea ice/three-dimensional ocean model. These experiments are (1) "cooling without freshening" and (2) "warm climate with freshening." The "cooling without freshening" results are split into two sections. First, we discuss the circulation characteristics during cold periods (section 3.1), and second we discuss the variability in some "cooling without freshening" experiments (section 3.2). In section 3.3 we discuss the results of our "warm climate with freshening" experiments.

3.1. Cooling Without Increased Freshwater Forcing

[25] Our first "cooling without freshening" experiment is a warm climate experiment to simulate a present day climate (control). In subsequent experiments we cool the atmosphere by increasing the planetary emissivity from e = 0.71 (warm) to e = 0.85 (cold). We use the freshwater forcing shown in Figure 1 for all of the "cooling without freshening" experiments. We perform various long (several thousand years) integrations to ensure proper statistical thermodynamic equilibrium.

[26] Figures 2, 3 and 4 show the equilibrium results of six progressively colder experiments. The top left panels of Figures 2, 3 and 4 show the warmest experiment (e = 0.71) and the bottom right panels show the coldest experiment (e = 0.85). The emissivity (e) for each experiment is given above each panel. Figure 2 shows a middle-longitude slice of the meridional overturning circulation (velocity vectors). Figures 3 and 4 show sea ice and sea surface density.

[27] In some of these experiments the circulation is variable (discussed in section 3.2). When variability is present, Figures 2 through 4 show the equilibrium results for the circulation at the weakest point in a cycle.

3.1.1. High-Latitude Sinking

[28] Figure 2 shows velocity vectors for the middle-longitude meridional overturning circulation in the warmest experiment (e = 0.71). In this experiment deep water forms at the northern boundary and penetrates to the bottom of the basin. There is no permanent sea ice (Figure 3, e = 0.71) and the sea surface density is highest along the northern boundary of the basin (Figure 4, e = 0.71). The lowest sea surface temperature is confined to a narrow region along the northern boundary (not shown). This circulation is similar to today's warm Holocene climate with strong stable deep water formation at northern latitudes.

3.1.2. Midlatitude Sinking

[29] In experiments with a colder atmosphere, the sinking region (at this middle-longitude location) shifts southward (Figure 2, e = 0.72 to e = 0.80), and there is weak penetration of the sinking water to the bottom of the basin. Most of the southern shifted circulation occurs above 2500 m. Figure 3 shows the sea ice for our six progressively colder experiments. In the warmest experiment (e = 0.71) there is no sea ice. In colder climates sea ice forms and expands southward. The highest density region also shifts southward below the southern boundary of the sea ice (Figure 4, e = 0.72 to e = 0.80) and the region of constant temperature near freezing surface water expands southward with the sea ice (not shown).

[30] The gradual southward shift of the deep water formation region, and weaker depth penetration of the sinking water, is essentially as some might expect for a glacial climate [*Keigwin and Lehman*, 1994; *Sarnthein et al.*, 1995; *Clark et al.*, 2002]. When the atmosphere is cold, northern latitudes also become less saline (not shown), because the weaker overturning circulation brings less high-salinity water northward [*Bryan*, 1986; *Manabe and Stouffer*, 1988]. In summary, in a colder climate sea ice expands southward, high-latitude surface waters freshen and the thermohaline circulation weakens. Some of these cold results also exhibit millennial period variability (discussed in section 3.2).

3.1.3. Low-Latitude Sinking

[31] In the coldest experiment (Figure 2) there is weak sinking in the southern part of the basin, and no deep water or intermediate water formation. Sea ice covers almost half of the basin (Figure 3, e = 0.85) and the highest density region is along the southern boundary (Figure 4, e = 0.85). High-salinity water in the south (not shown) drives the weak reverse-overturning circulation. There is no evidence of these extreme cold conditions and or deep water formation in the tropics in the geologic record for the last glacial period. So, although this may be a possible circulation mode it is unlikely that such a circulation pattern occurred during the last glacial period or during the Holocene.

3.2. Variability in "Cooling Without Freshening" Experiments

[32] Perhaps the most interesting aspect of these experiments is the robust presence of millennial-scale oscillations in the temperature and salinity throughout the basin pro-

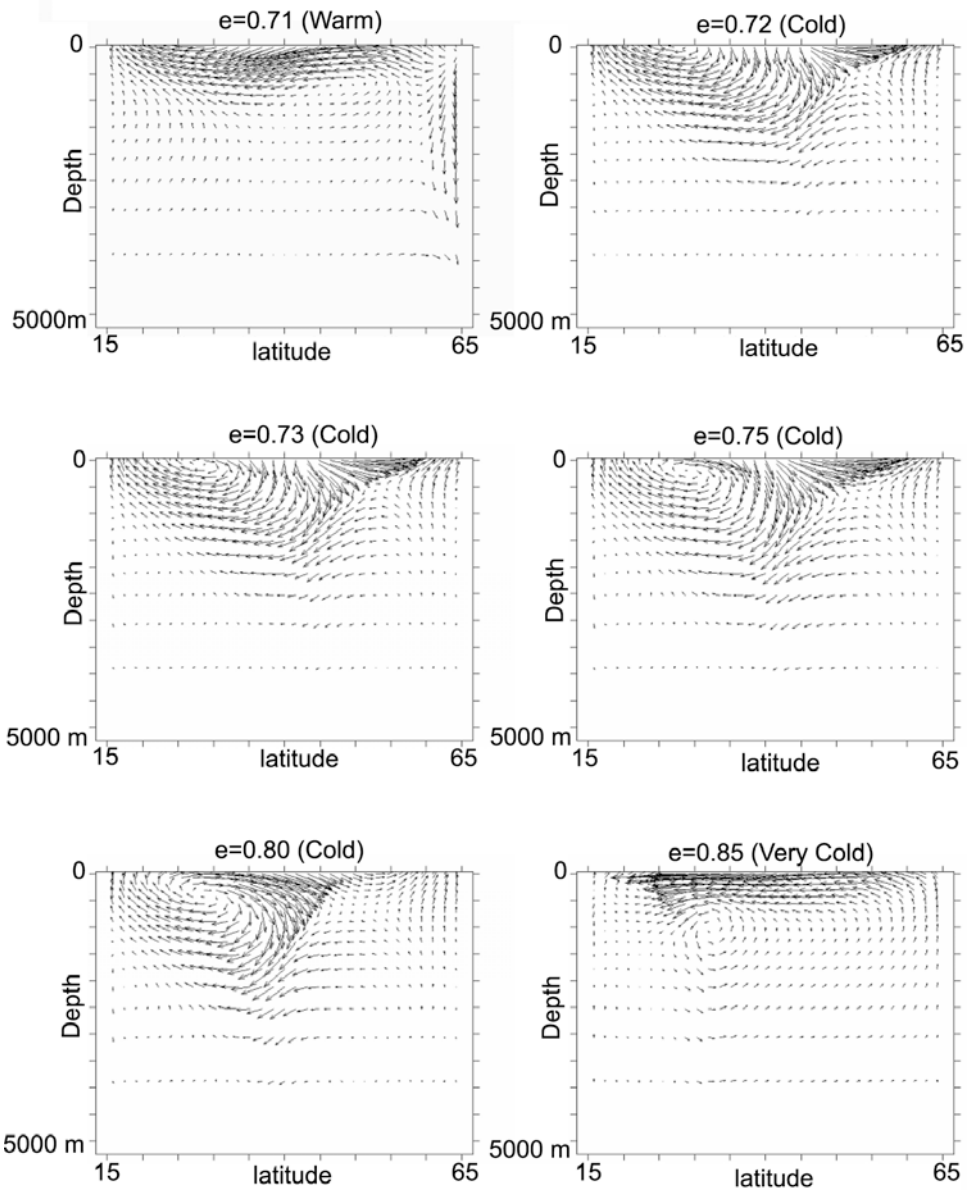

Figure 2. Velocity vectors of middle-longitude meridional overturning circulation in "cooling without freshening" experiments. The top left panel shows the warmest control experiment (e = 0.71) where there is deepwater formation at the northern boundary of the basin. In colder experiments (e = 0.72 to 0.80) the sinking region shifts southward, and the sinking shoals. In the coldest experiment (e = 0.85), there is weak sinking in the southern part of the basin.

duced by changes in the strength of the overturning circulation. These oscillations have many of the characteristics of Dansgaard-Oeschger cycles, as we now describe.

3.2.1. Atmosphere Temperature

[33] One of the distinguishing characteristics of Dansgaard-Oeschger events is their sawtooth-shaped temperature profile [*Dansgaard et al.*, 1993; *Bender et al.*, 1994]. Figure 5 shows high-latitude atmosphere-temperature time series for our six progressively colder experiments. In Figure 5 (e = 0.73) the sawtooth-shaped pattern of rapid warming, followed by slow cooling, and finally rapid cooling, is apparent in many of the short-duration modeled warming events. The longer high-amplitude warm events have a flat top (only slightly sloped). The high-latitude atmospheric temperature change for the modeled Dansgaard-Oeschger cycles is about 15°C to 20°C, which is comparable to, if slightly higher than what ice core evidence suggests [*Johnsen et al.*, 1992; *Taylor et al.*, 1993]. (The amplitude of modeled high-latitude temperature change varies with the magnitude of the ice-albedo feedback.)

[34] In one typical integration, with e = 0.73, warm periods occur approximately every 2500 years, with higher-amplitude warm events at roughly 7000-year intervals. There are no oscillations in the warmest control

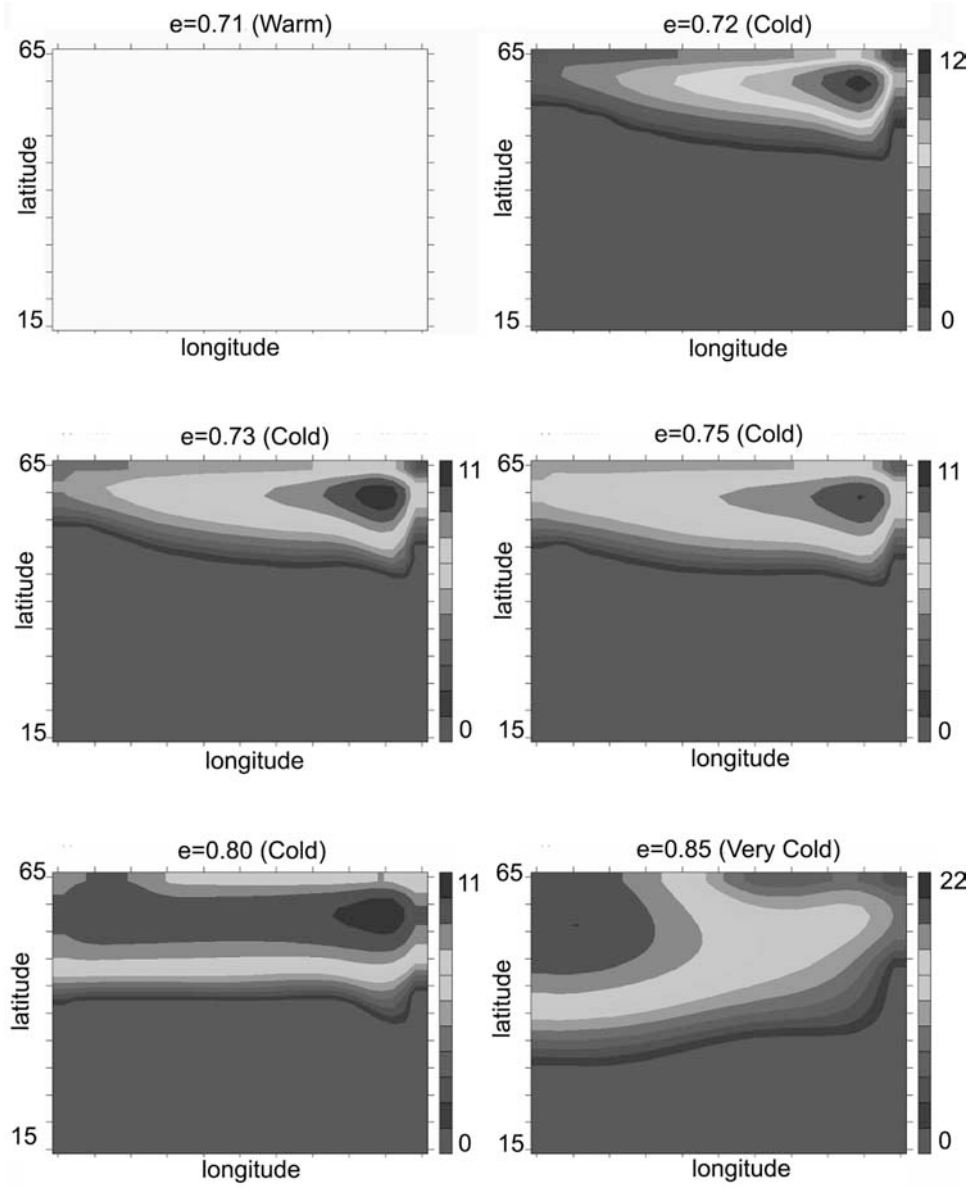

Figure 3. Sea ice thickness and extent for ''cooling without freshening'' experiments. In the warmest experiment (e = 0.71), there is no sea ice. In the cold experiments (e = 0.72 to 0.85), sea ice forms and expands. In the coldest experiment (e = 0.85), sea ice covers almost half of the basin. The region of constant temperature, near-freezing, surface water expands with the sea ice edge (not shown). See color version of this figure at back of this issue.

experiment (e = 0.71) and there are only very low amplitude oscillations in the coldest experiment (e = 0.85). The approximate periods for warm events (~2500 years), and for high-amplitude warm events (~7000 years), are broadly consistent with the evidence from ice cores for Dansgaard-Oeschger events [*Johnsen et al.*, 1992; *Bender et al.*, 1994; *Bond et al.*, 1997; *Severinghaus et al.*, 1998; *Bianchi and McCave*, 1999].

[35] The sawtooth temperature profile at high latitudes results from changes in the surface radiative forcing (surface albedo and insulating effect of ice) when sea ice melts and forms. During a warming event, the ice thins and no longer insulates the warmer ocean from the atmosphere; under these conditions the remaining sea ice melts rapidly, and the surface warms rapidly, aided by the decrease in surface albedo. In contrast, after a warming event, the circulation only slowly diminishes and sea ice builds up only gradually, with correspondingly slow surface cooling. Once the sea ice is thick enough to insulate the ocean from the atmosphere, the surface cools more rapidly, causing the abrupt cooling at the end of a cycle. The temperature changes abruptly at northern latitudes, where sea ice is melting and freezing, and changes more gradually at ice-free southern latitudes [*Gildor and Tziperman*, 2003; *Kaspi et al.*, 2004].

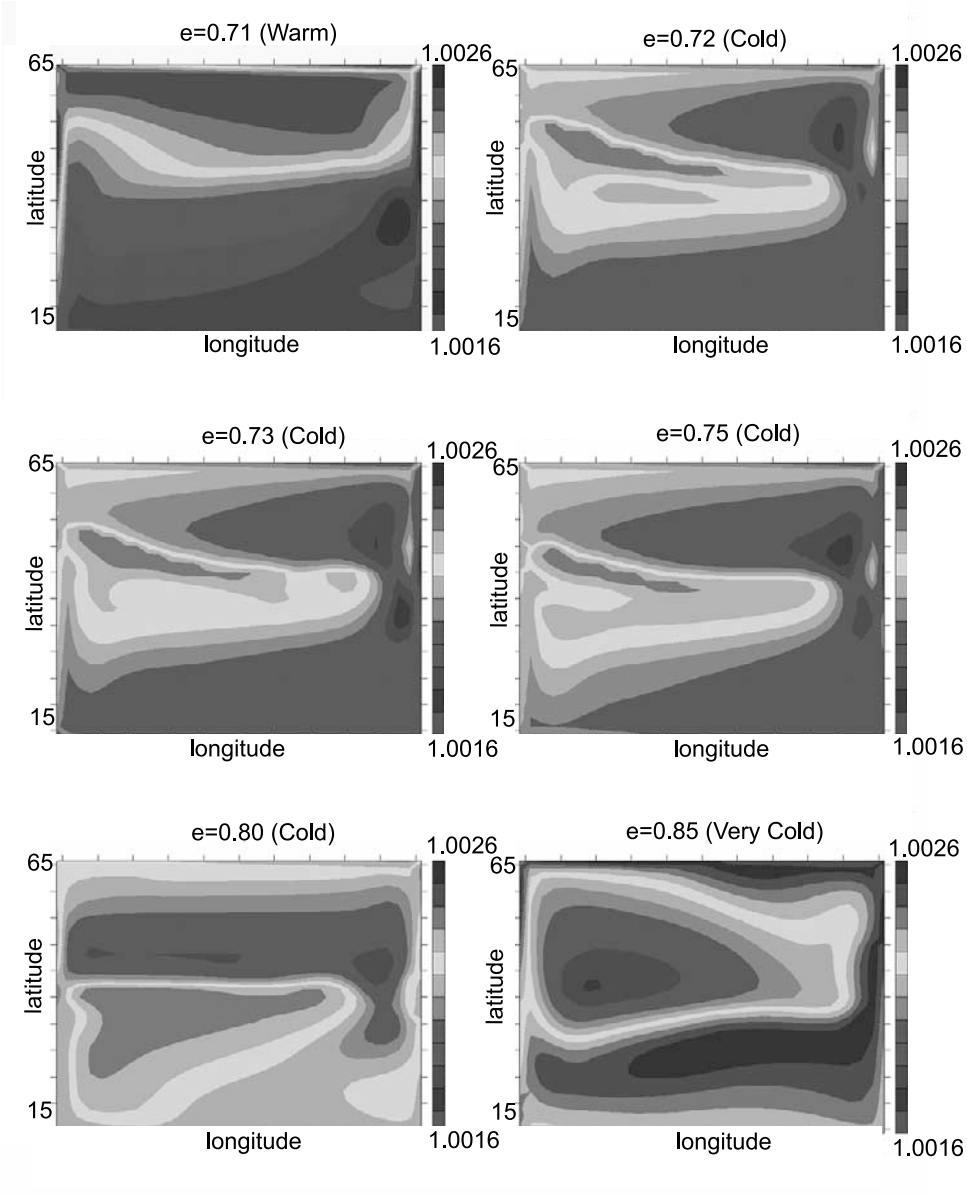

Figure 4. Surface density for "cooling without freshening" experiments. In the warmest experiment (e = 071) the highest density water is along the northern boundary where deep water is forming. In the cold experiments (e = 0.72 to 0.80) the sinking region shifts southward. In the coldest experiment (e = 0.85) the highest-density water is along the southern boundary, and there is weak reverse overturning. See color version of this figure at back of this issue.

[36] Figure 6 shows a high- and low-latitude atmosphere temperature profile for two warm events in the e = 0.73 experiment. The temperature change at high latitudes is more abrupt and higher amplitude than the temperature change at low latitudes. This is consistent with *Blunier et al.*'s [1999] findings that Dansgaard-Oeschger events are smaller amplitude outside of the North Atlantic region and the distinct sawtooth profile is most apparent in proxies from northern latitudes [*Broecker and Hemming*, 2001].

3.2.2. Sea Surface Temperature

[37] Figure 7 (left) shows a time series of high-latitude and low-latitude sea surface temperature and high-latitude deep-ocean temperature for the e = 0.73 experiment. The high-latitude sea surface temperature changes about 1°C over the first oscillation and almost 5°C over the second oscillation, agreeing with estimates of 2° to 5°C for Dansgaard-Oeschger events [*Bond et al.*, 1993]. At low latitudes and in the deep ocean sea surface temperature changes approximately 2°C over one oscillation. The deep ocean warms gradually between high-latitude warming events and cools rapidly when the high-latitude temperature increases. At low latitudes, the sea surface temperature change is more gradual and generally lower amplitude. The sea surface is warm in the south when the high-latitude

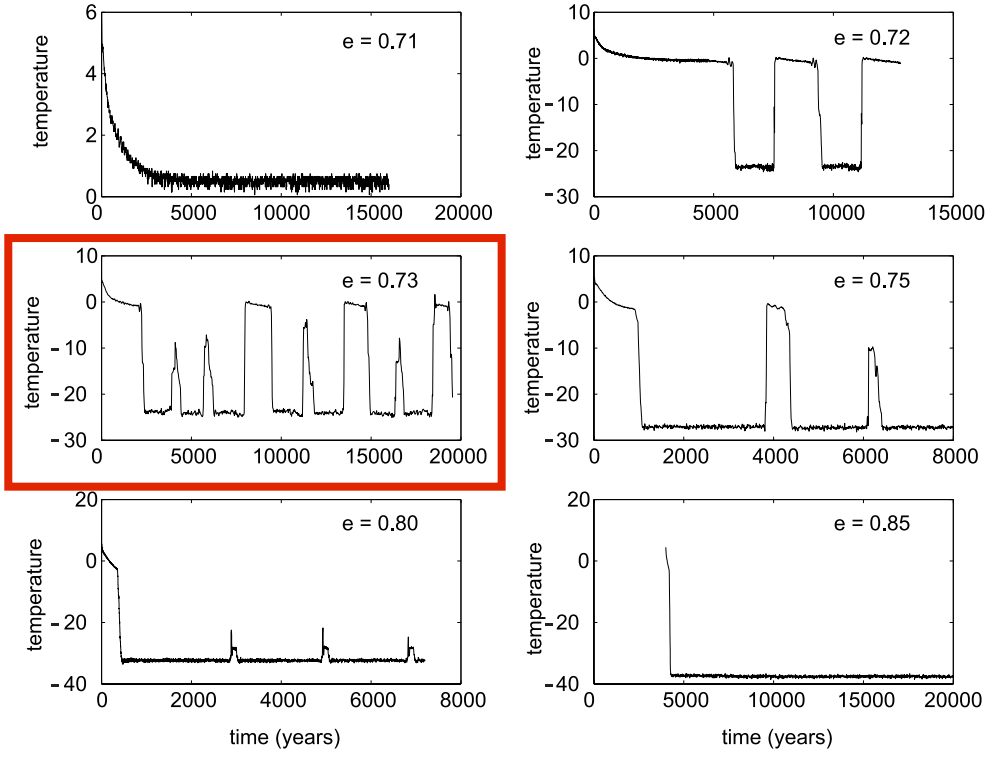

Figure 5. High-latitude atmosphere temperature time series for the "cooling without freshening" experiments. In the experiments with emissivity between e = 0.72 and e = 0.80 the climate is cold, sea ice forms, and the high-latitude atmosphere temperature oscillates with a period of a few thousand years.

surface is cool and vice versa, creating a "seesaw" effect [*Pflaumann et al.*, 2003].

[38] An interesting feature of modeled oscillations is the magnitude of temperature change in the deep ocean; the high-latitude deep-ocean temperature change is comparable to the surface ocean temperature change (Figure 7). This result suggests that reconstruction of glacial deep-ocean temperature variability would be a useful test of the mechanisms suggested in this paper.

3.2.3. Sea Surface Salinity

[39] Figure 7 (right) shows a time series of high-latitude and low-latitude sea surface salinity and high-latitude deep-ocean salinity in the e = 0.73 experiment. During warming events the high-latitude salinity increases abruptly while the deep-ocean and low-latitude surface salinity decrease slightly. The salinity at high latitudes increases almost one salinity unit over one oscillation because of northward flux of high-salinity water during a rapid overturning event. Salinity changes in the deep ocean are much smaller amplitude (about 0.1 salinity unit over a single oscillation).

3.2.4. Meridional Overturning Circulation

[40] Figure 8 (top) shows a time series of oceanic (red) and atmospheric (blue) meridional heat transport at approximately 50°N (top) and 40°N (center). Figure 8 (bottom) shows the maximum overturning circulation in sverdrups (red) and the sea ice thickness (blue) at a mid basin location near 50°N. The maximum overturning occurs at about 50°N and at a depth of about 3700 m.

[41] The maximum overturning circulation is very weak between warming events (~0.5 Sv) and increases to over 18 Sv during a warming cycle. Thus a significant increase in maximum overturning circulation accompanies the warming events illustrated in Figures 6 and 7. For comparison, the overturning circulation calculated by this model for a Holocene climate (not shown) with stable deep water formation (e = 0.71) is about 15 Sv.

[42] The 50°N location (Figure 8, top) is near the sea ice edge (see Figure 3). Because of this the temperature gradient in the atmosphere is very large but the ocean surface is near the freezing point so the ocean surface forcing gradient is flattened. Virtually all of the northward heat transport takes place in the atmosphere, with much smaller northward heat transport by the ocean.

[43] In the first rapid overturning event at 50°N (5400–6000 years) the northward heat transport (Figure 8, top) increases in both the ocean (red) and atmosphere (blue). During this event the sea ice does not completely melt (Figure 8, bottom) so the ocean and atmosphere remain insulated from each other and the ocean surface forcing gradient remains flattened. Northern latitude locations warm and southern latitude locations cool slightly during this event as seen in Figures 6 and 7.

[44] In the second higher-magnitude warming event (around 7600 years) at 50°N the oceanic heat transport (red) increases over the entire warming cycle but the atmospheric heat transport (blue) increases only initially.

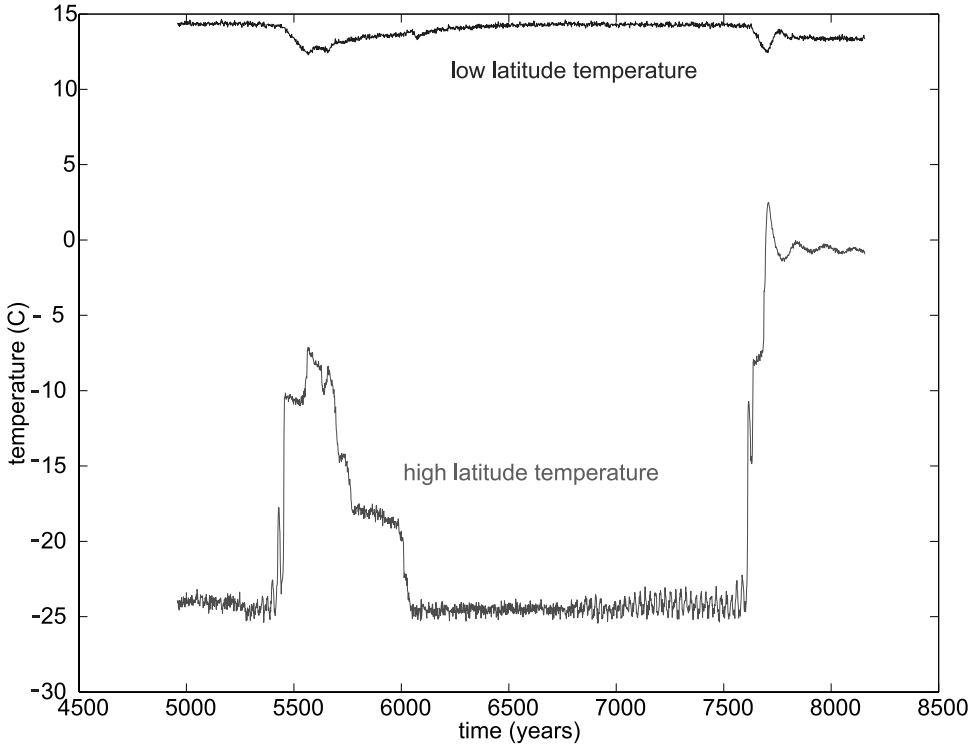

Figure 6. Atmosphere-temperature time series for two warm events in the e = 0.73 "cooling without freshening" experiment. The high-latitude atmosphere temperature change is out of phase with the low-latitude temperature change. The low-latitude temperature change is gradual, and the temperature change at high latitudes is more abrupt and higher amplitude. The small-amplitude warm event displays the distinct sawtooth profile for the high-latitude atmosphere temperature. See color version of this figure at back of this issue.

Once the sea ice completely melts, the atmospheric heat transport is reduced over most of the later part of the second warming cycle. When sea ice completely melts, rapid switches in meridional heat flux (Figure 8, top) and temperature (Figure 7) occur because the ocean surface temperature forcing gradient increases dramatically.

[45] At the 40°N location there is no sea ice and the atmosphere heat transport is comparable to, although still larger than, the oceanic heat transport. Here the northward heat transport (Figure 8, center) increases in the ocean and decreases in the atmosphere during both warming events. The reduction in atmospheric heat transport corresponds to a reduction in the atmospheric temperature gradient (Figure 6). Northern latitudes warm and southern latitudes cool during rapid overturning events as seen in Figures 6 and 7. The increased northward mass transport by the ocean (Figure 8, bottom) increases the northward transport of heat by the ocean (Figure 8, center).

[46] To explain the reason for the variability in our cold climate simulations, consider the mechanisms of maintaining the thermohaline circulation. The overturning circulation in a basin is particularly sensitive to the surface heat flux at high-latitudes, in the subpolar gyre, because it is buffered from the surface conditions in the subtropical gyre by the presence of a near isothermal base to the ventilated thermocline [*Samelson and Vallis*, 1997]. Consistently, *Winton* [1995] found that a high-latitude cover of sea ice, which inhibits heat loss at the ocean surface, leads to weaker thermohaline circulation. Typically, a weak thermohaline circulation is more susceptible to variability [*Tziperman*, 1997] essentially because, in a weak circulation, there is a closer balance between the competing effects of diffusion and advection, and diffusion can warm and destabilize the abyss. (Figure 7 shows the slow diffusive warming of the deep ocean between warming cycles.) Thus the weak overturning is unstable on the millennial timescale, and occasionally spontaneously transitions to a stronger circulation, with higher temperatures at northern latitudes, that may last for several hundred years. However, the strong circulation cannot be sustained, and the climate slowly reverts to the weaker thermohaline state with lower temperatures. This hypothesis is qualitatively consistent with the geologic record and is a possible explanation of the high-amplitude temperature variability during cold periods.

3.2.5. Characteristics of One Cycle

[47] For analysis of the physical characteristics of these modeled warming events, we plot snapshots of various parameters (velocity vectors, sea surface temperature and sea surface salinity) at strong and weak circulation stages of an oscillation. Figure 9 shows middle-longitude meridional slices of the overturning circulation (velocity vectors) for

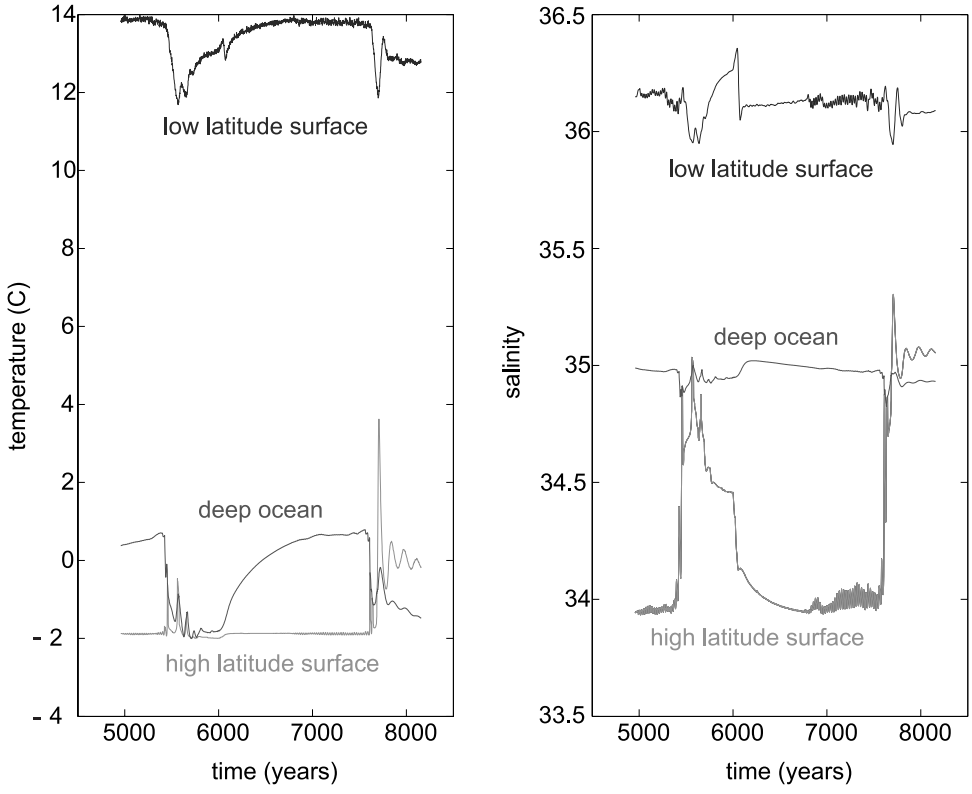

Figure 7. Time series of high-latitude, low-latitude and deep ocean temperature and salinity for the e = 0.73 experiment. (left) The high-latitude sea surface temperature changes by a few degrees over a single oscillation. At low latitudes and in the deep ocean, sea surface temperature changes are smaller. During warm events the (right) high-latitude salinity increases abruptly while the deep ocean and low-latitude surface salinity decreases. See color version of this figure at back of this issue.

each of our snapshot times. During the weakest point in the overturning circulation (Figures 9a and 9c) northern sinking deep water formation is absent, and is replaced by increased southern sinking intermediate water. This occurs because the sinking region is closer to the boundary between the subpolar and subtropical gyre, and thus is influenced by Ekman pumping, entraining some of the sinking water into the main thermocline and the intermediate water below. When the circulation is strong, the deep water formation shifts to the north (Figure 9b) and the circulation is as might be expected during the Holocene.

[48] In these experiments, the ocean circulation oscillates between strong convection at the northern boundary (Figure 9b) and weaker midlatitude convection (Figures 9a and 9c). The changes in position and depth of the overturning circulation over one modeled cycle are typical of the circulation changes expected during a cold glacial climate [*Boyle and Keigwin*, 1987; *Duplessy et al.*, 1988; *Oppo and Lehman*, 1995; *Sarnthein et al.*, 1995; *Bigg et al.*, 2000]. In particular, our modeled glacial circulation is consistent with Oppo and Lehman's finding that, during the glacial period, warm events were accompanied by increases in North Atlantic Deep Water production, and is consistent with the finding that North Atlantic Deep Water production was replaced by increased southern sinking intermediate water during cold periods [*Boyle and Keigwin*, 1987; *Dansgaard et al.*, 1993; *Oppo and Lehman*, 1995].

[49] Figures 10a–10c show snapshots of sea surface temperature over one cycle. During the weakest point, northern sea surface temperature is low and the cold region extends to about the middle of the basin. During an increased overturning event (Figure 10b), the northern ocean warms, the southern ocean cools and the region of very low temperature in the north shrinks to about half. In Figure 10c, the region of low sea surface temperature expands southward, returning to the original state. Thus the conditions in the modeled North Atlantic oscillate between a warm climate with high-latitude sinking, which is similar to or slightly cooler than the present day Holocene climate, and a cold glacial climate with midlatitude sinking.

[50] Figures 10d–10f show sea surface salinity snapshots over one cycle. At the weakest point (Figure 10d), low-salinity water pools over northern latitudes. During a rapid overturning event, the range of sea surface salinity is reduced; high latitudes become more saline and low latitudes become slightly less saline. This is consistent with northern latitude freshening during cold periods found by various workers [*Duplessy et al.*, 1991; *de Vernal and Hillaire-Marcel*, 2000; *de Vernal et al.*, 2000]. Some theo-

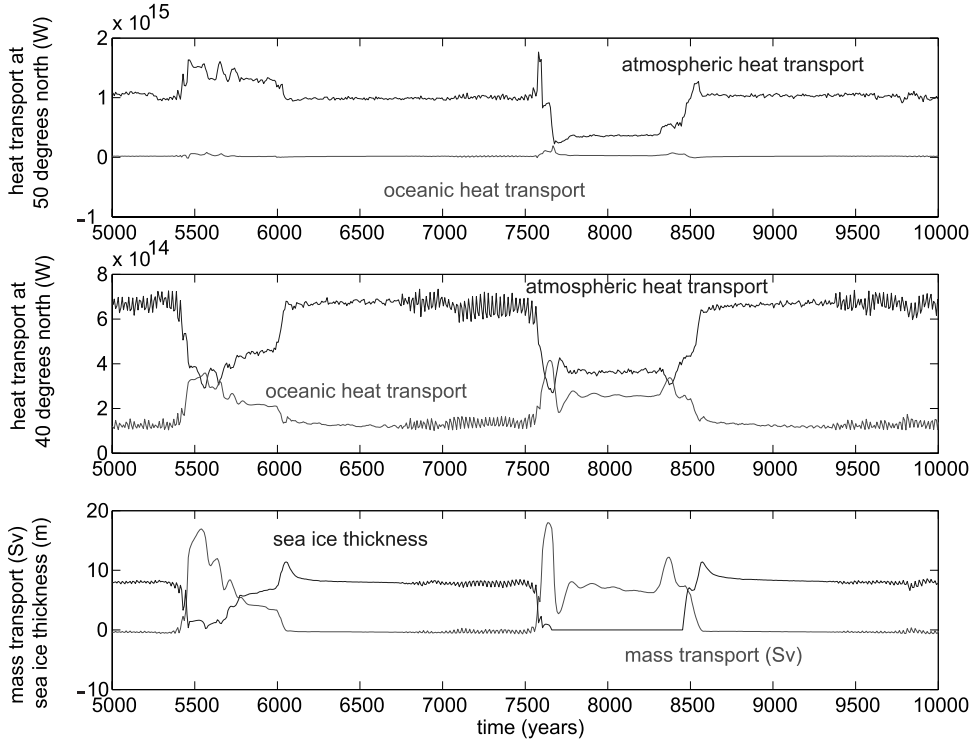

Figure 8. Time series of oceanic (red) and atmospheric (blue) meridional heat transport at (top) 50°N and (center) 40°N. (bottom) Maximum overturning circulation in sverdrups (red) and sea ice thickness (blue). The oceanic heat transport (red) increases over both warming cycles at 40°N, and the atmospheric heat transport (blue) decreases. (top) The increase in meridional heat transport by the ocean is accompanied by (bottom) an increase in mass transport by the ocean. The reduction in heat transport by the atmosphere is associated with a reduction in the atmospheric temperature gradient (Figure 6). The (top) 50°N location is near the sea ice edge where the meridional temperature gradient in the atmosphere is very large. See color version of this figure at back of this issue.

ries, such as the salt oscillator hypothesis, predict that lowered sea surface salinity, due to oscillations in continental ice, caused cooling cycles during the last glacial period [*Broecker et al.*, 1990; *MacAyeal*, 1993]. In some contrast, our results suggest that southward expansion of sea ice caused weakness and variability in the thermohaline circulation during the last glacial period, and lowered sea surface salinity occurred during the weak stage in the variable circulation.

3.3. "Warm Climate With Freshening"

[51] In these experiments we explore changes in the ocean circulation which occur with increased freshwater forcing in a warm climate. As in our cooling experiments we start with the warm control experiment where e = 0.71 (Holocene climate) but here we increase the latitudinal freshwater forcing without changing the temperature forcing (emissivity held constant). We conduct four experiments where we increase the freshwater forcing by multiplying the baseline freshwater flux (Figure 1) by 1.3, 1.6, 2.0 and 4.0.

[52] Figure 11 shows a middle-longitude slice of meridional overturning circulation (velocity vectors) for our four "warm climate with freshening" experiments. The multiplier for the baseline freshwater forcing is shown above each panel. The radiative forcing in all of these experiments is that of a warm Holocene climate.

3.3.1. High-Latitude Sinking

[53] There are no oscillations in our warm climate experiments. In all four "warm climate with freshening" experiments the circulation reaches a steady state after about 2500 years. High-latitude convection is present in all but the freshest of these experiments (4.0×, Figure 11). This strong high-latitude convection is representative of the circulation expected in a warm Holocene climate. Eventually, the freshwater forcing becomes high enough (4.0×) to shift the circulation to salinity-driven reverse overturning.

3.3.2. Midlatitude Sinking

[54] In these warm climate results, the circulation never shifts to midlatitude sinking as it did in our cold climate experiments and there is no millennial period variability.

[55] Increased freshening in a warm climate produced results that are very different from the "cooling without freshening" results and our "warm climate with freshening" results do not match the geologic record for the last glacial period. Specifically, there is no evidence for reverse

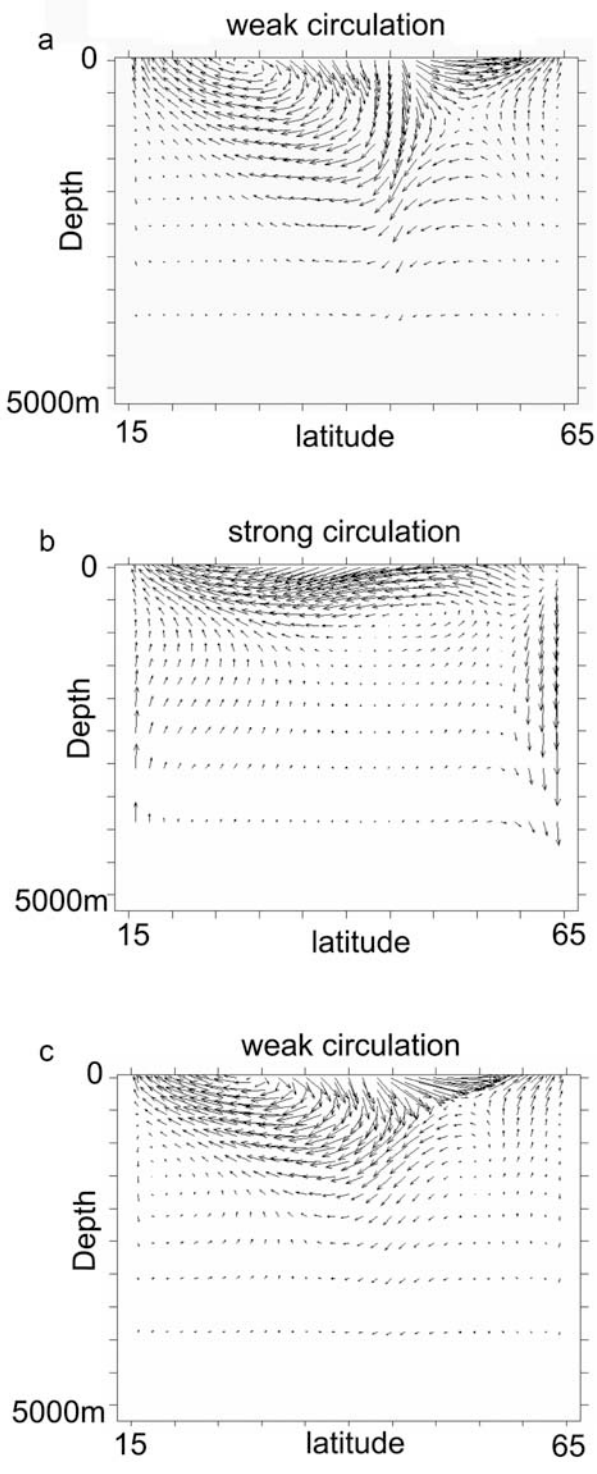

Figure 9. Middle-longitude velocity vectors for meridional overturning circulation at various times over one cycle for the e = 0.73 ''cooling without freshening'' experiment. The model oscillates between weak southern-shifted overturning and strong northern sinking. (a) and (c) Weakest point in the overturning circulation where the sinking region is shifted southward and there is weak penetration of deep water to the bottom of the basin. (b) Strong overturning circulation with deep water formation at the northern boundary.

overturning in recent times or during the last glacial period and we expect that such extreme surface conditions are unlikely for either of those periods.

4. Four-Box Coupled Model Experiments

[56] To further explore the robustness of our results, we conducted two sets of similar experiments with our four-box ocean model. The simplicity of the box model helps to show clearly why midlatitude sinking is present in the ''cooling without freshening'' results and absent from the ''warm climate with freshening'' results. There is no variability in our box model results, but the circulation changes that weaken meridional overturning and lead to variability are similar in both the box model and the three-dimensional model results.

4.1. "Cooling Without Freshening": Box Model Results

[57] In our box model ''cooling without freshening'' experiments we cool the atmosphere by reducing the atmosphere restoring temperature (T_{hres}, T_{lres}) while holding the surface temperature gradient constant ($T_{hres} - T_{lres}$ = 36 K). In these experiments the freshwater forcing (Fs) is constant at 0.55 m yr^{-1}. Figure 12 (top) shows the density (''y'' axis) for all four ocean boxes in the box model ''cooling without freshening'' experiments. The ''x'' axis is the high-latitude atmosphere restoring temperature (T_{hres}).

4.1.1. Results

[58] When the high-latitude restoring temperature is above 259 K, the high-latitude surface box (magenta) is the densest box (Figure 12, top). Since the deep-ocean box (green) is less dense, convection is occurring between the high-latitude and deep-ocean box. This circulation pattern is present when boundary conditions most like those expected during a Holocene climate are applied [*Sarnthein et al.*, 1995].

[59] When the high-latitude restoring temperature falls below 259 K the midlatitude box (red) becomes the densest so there is convection between the midlatitude and deep-ocean boxes. When the high-latitude restoring temperature is around 258 K, the high-latitude box (magenta) becomes completely covered by sea ice, and sea ice starts to form on the midlatitude box (red).

[60] In experiments with a very cold atmosphere, the midlatitude box becomes completely covered in ice ($\sim$244 K), and the low-latitude box (blue) becomes the densest. In this very cold state, the temperature driven northern and midlatitude sinking ceases and salinity driven low-latitude sinking occurs.

[61] In each colder experiment, sea ice expands and the four-box model circulation progresses from northern sinking, to midlatitude sinking and finally to reverse overturning. This is consistent with the circulation pattern of our three-dimensional results [*Boyle and Keigwin*, 1987; *Duplessy et al.*, 1988].

4.1.2. Sea Ice Role

[62] It is the expanding sea ice that causes the box model circulation changes because it results in an effective decrease in the ocean surface temperature forcing (even though the gradient of the atmosphere temperature forcing

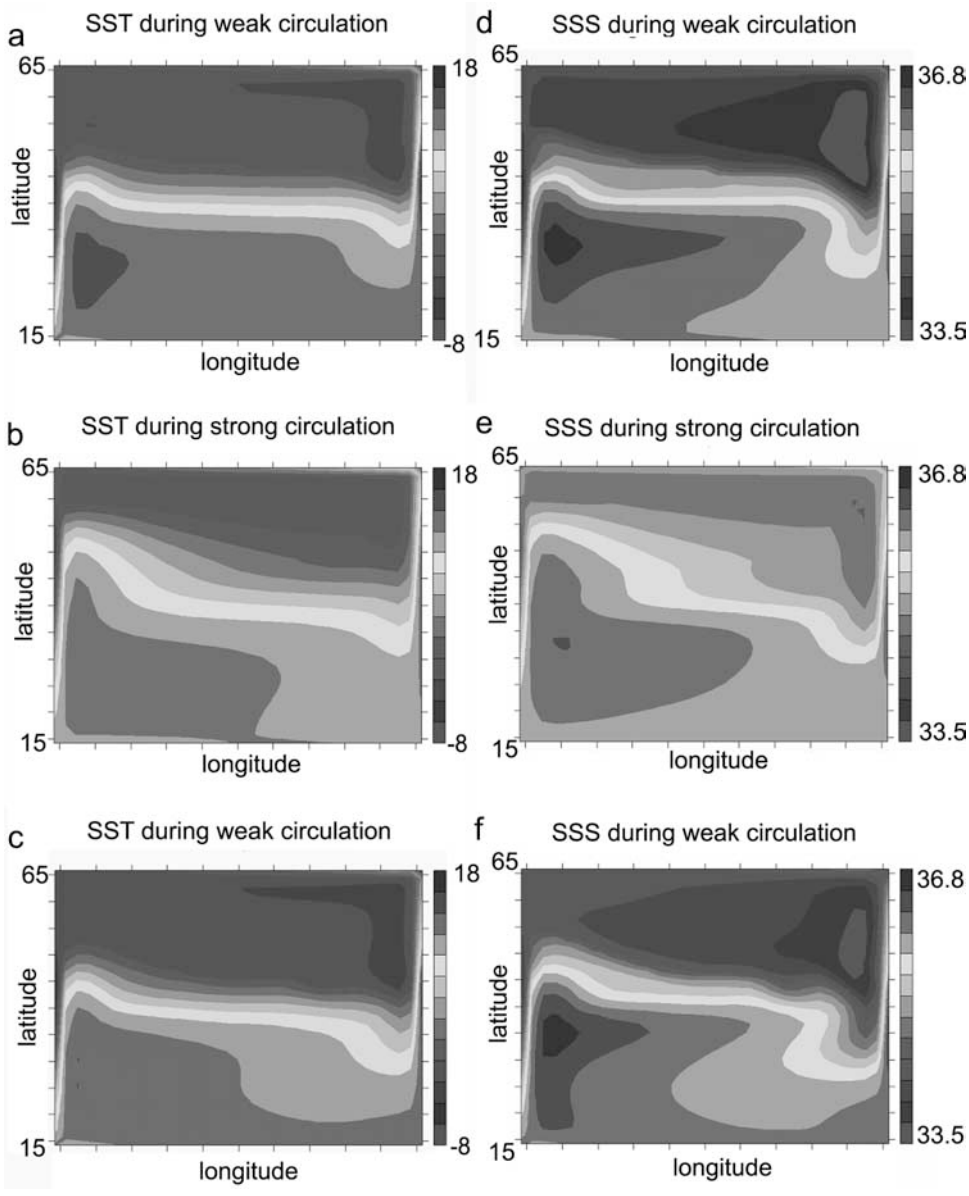

Figure 10. Sea surface temperature and salinity at various times over one cycle for the e = 0.73 experiment. (a) SST at the weakest point in the circulation. The cold region in the north extends to about the middle of the basin. (b) SST for a strong circulation. Note the northern ocean warms and the southern ocean cools. (c) SST with the circulation in its weak phase again. (d–f) Sea surface salinity during periods corresponding to Figures 10a–10c. During weak periods in the circulation (Figures 10d and 10f) the high-latitude sea surface freshens. See color version of this figure at back of this issue.

remains constant). To understand why, consider the case where the high-latitude box is completely covered in ice. Further reduction in the atmosphere temperature does not change the restoring temperature of the high-latitude box because the ocean temperature cannot drop below the freezing point; however, the midlatitude and low-latitude boxes can continue to cool toward the freezing point. This ''flattens'' the temperature gradient at high-latitudes and reduces the overall forcing temperature gradient at the ocean surface. In the extreme cold case, all of the surface boxes would be covered in ice and the temperature gradient at the surface of the ocean would be zero. In this case, the surface forcing would depend purely on the freshwater forcing gradient (E−P).

[63] We find a similar result with the three-dimensional model. Cooling the atmosphere (when sea ice is included) fixes the ocean restoring temperature, in ice covered regions, at 271 K. This causes a flattening of the temperature gradient at high latitudes, and an overall reduction in the gradient of the temperature forcing at the surface of the ocean. The sinking region shifts southward of the constant temperature region, and weakens and destabilizes the deep circulation, leading to the modeled Dansgaard-Oeschger-like cycles.

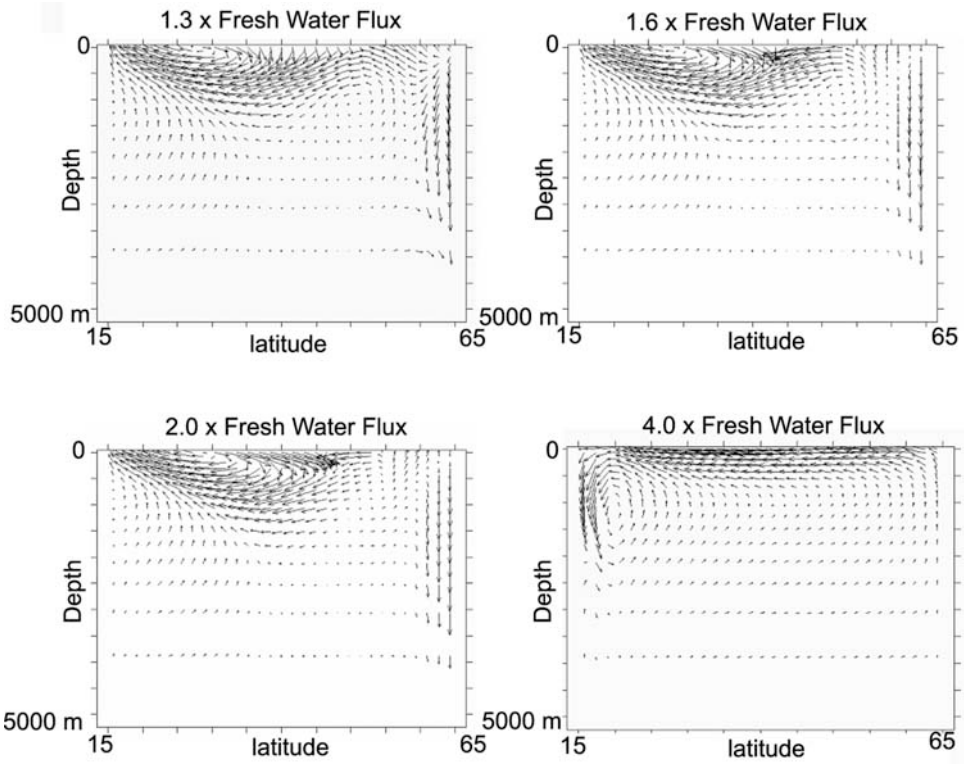

Figure 11. Middle-longitude velocity vectors for meridional overturning circulation in the "warm climate with freshening" experiments. Figure 11 shows the results of experiments where we start with a warm climate (e = 0.73) and increase the surface freshwater forcing by multiplying the baseline forcing by 1.3, 1.6, 2.0 and 4.0. All of these warm experiments (except the times 4.0× experiment) have strong deep water formation at the northern boundary and no oscillations. In the 4.0× experiment, there is weak reverse overturning circulation.

4.2. "Warm Climate With Freshening": Box Model Results

[64] In these experiments the high-latitude restoring temperature (T_{hres}) is set to 264 K, and the low-latitude restoring temperature (T_{lres}) is set to 300 K to simulate a warm climate. Instead of cooling the atmosphere, we increase the freshwater forcing (F_s) from 0.55 m yr^{-1} to a maximum of 1.80 m yr^{-1}.

[65] When the freshwater forcing is between 0.55 and 1.60 m yr^{-1} (Figure 12, bottom), the high-latitude box is the densest and strong convection is occurring between the high-latitude box and the deep-ocean boxes. When the freshwater forcing is greater than 1.6 m yr^{-1}, the low-latitude box becomes the densest, and reverse salinity-driven convection sets in.

[66] In our models only cold conditions, with expanded sea ice, produce the midlatitude convection which may have existed during the last glacial period [*Boyle and Keigwin*, 1987; *Oppo and Lehman*, 1993]. Increasing salinity forcing in a warm climate causes the model to transition directly from high-latitude sinking to low-latitude sinking when salinity forcing reaches 1.6 m yr^{-1}. These differences are explained by the difference in the shape of the curve for surface temperature forcing and salinity forcing. The temperature forcing "flattens" at high latitudes as sea ice expands. The salinity forcing of the high-latitude box increases with respect to the low-latitude box. We have not conducted experiments with a "flattened" high-latitude salinity gradient because there is no obvious natural mechanism for prolonged flattening of the high-latitude salinity gradient in the North Atlantic Ocean. Thus there is no shift to midlatitude sinking in the "warm climate with freshening" experiments as in the "cooling without freshening" where the ocean surface temperature forcing gradient flattens naturally because of expanded sea ice.

5. Conclusion and Discussion

[67] In this paper we have explored mechanisms for glacial climate variability using a three-dimensional ocean model coupled to an energy balance atmosphere, and using a simpler ocean box model. We find that cooling alone, with no additional forms of external forcing or variability, leads to a climate with two of the most significant features of the observed glacial climate:

[68] 1. The glacial climate is less stable and is characterized by intermittent, millennial-scale oscillations similar in many ways to Dansgaard-Oeschger cycles.

[69] 2. The glacial ocean circulation is generally weaker with shallower Northern Hemisphere overturning, and the deep water formation region is shifted equatorward of the present sinking region.

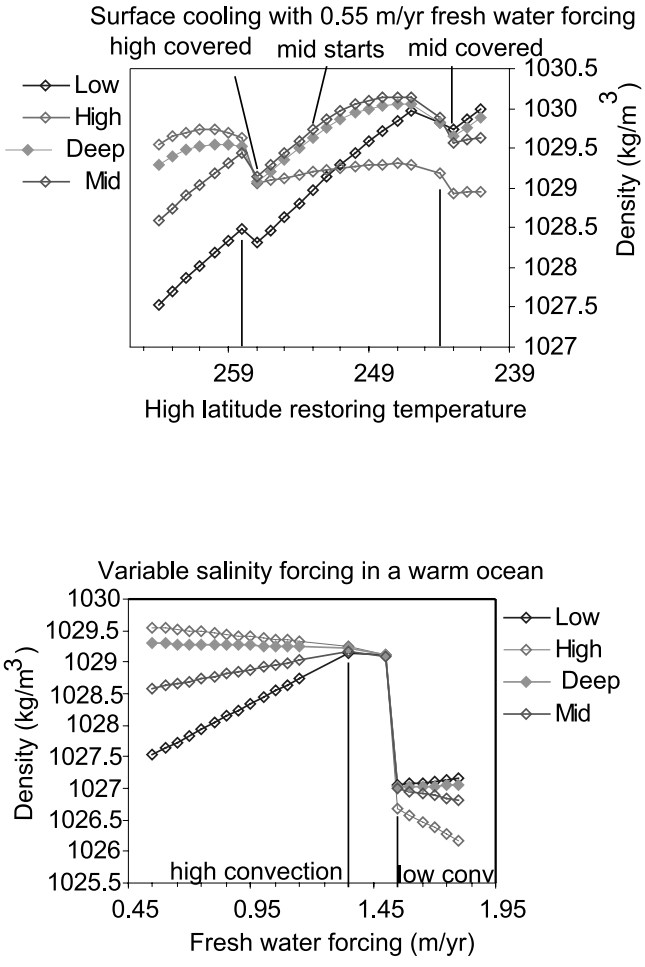

Figure 12. Four box model results. (top) Density against high-latitude restoring temperature for each box in the "cooling without freshening" experiments. In these experiments the circulation transitions from high-latitude convection to midlatitude convection and finally to low-latitude convection. (bottom) Density for each box in experiments where we increased the high-latitude freshwater forcing in a warm climate. The shift to midlatitude convection does not occur in these warm climate results, and the circulation shifts directly from high- to low-latitude sinking when sufficient freshwater forcing is applied. See color version of this figure at back of this issue.

[70] Both of these features are a consequence of the growth of sea ice. Sea ice inhibits the loss of buoyancy at high latitudes and leads to a generally weaker and shallower overturning circulation with midlatitude (rather than high latitude) sinking near the edge of the ice sheet. (This is consistent with *Boyle and Keigwin*'s [1987] finding that North Atlantic Deep Water production was replaced by increased southern sinking intermediate water during cold periods.) This circulation is unstable, and millennial-scale oscillations are produced. During these events, the overturning circulation is much stronger and high latitudes are considerably warmer than normal for glacial periods.

[71] Sea ice also plays a role in the sawtooth-shaped atmospheric temperature profile which is apparent during overturning oscillations (Figure 6): Melting sea ice enhances rapid warming at the beginning of a cycle, and the meridional overturning circulation is able to quickly spin up and warm high latitudes. The subsequent cooling is more gradual, but the increase in albedo and the insulating effect of sea ice cause rapid cooling at the end of a warming cycle. That sea ice is important is consistent with the models of *Gildor and Tziperman* [2000] and *Kaspi et al.* [2004], in which sea ice switches enhance the abrupt atmospheric temperature changes at northern latitudes, where sea ice is melting and freezing.

[72] The simulated features of oscillations are generally consistent with observed Dansgaard-Oeschger cycles, and several aspects that both the model and observations have in common are (1) high-latitude sawtooth-shaped temperature profile, (2) warm events occurring approximately every 2500 years, (3) higher-amplitude warm events occurring approximately every 7000 years, (4) high-latitude sea surface temperature change of 2°C over a cycle, and (5) high-latitude atmosphere temperature change of the order of 15°C over a cycle.

[73] Of course, some of these numbers are dependent upon parameters in the model. For instance, when the diffusivity parameter is reduced the oscillation period lengthens (because it then takes longer to warm the deep ocean to the point of instability), but the period remains between 1000–3000 years over a broad range of diffusivity values. Nevertheless, it is notable that the model can reproduce many of the features of the observed glacial climate without additional external forcing and without excessive tuning.

[74] High-latitude freshening in a warm climate impacts the thermohaline circulation and climate very differently than overall cooling of the climate. In general, the high-latitude sinking in our warm climate integrations is very stable. From our three-dimensional results we estimate that, when the climate is warm, the freshwater forcing at the surface has to be quadrupled to cause a shift to weak reverse overturning. Furthermore, such freshening alone does not produce a shift to midlatitude sinking or variability such as occurred during glacial periods.

[75] We find that neither stochastic forcing (emulating weather) nor a seasonal cycle is necessary to produce variability in our experiments, but neither does their presence damp such variability. In particular, the millennial-scale variability is also present in experiments which include a seasonal cycle.

[76] Millennial variability is also present in experiments without stochastic forcing. Figure 13 shows a time series for temperature in the e = 0.73 experiment without stochastic forcing. Without stochastic forcing the warming events are more regular in period and amplitude. Stochastic forcing increases the amplitude variation for warming events causing the higher-amplitude warming events approximately every 7000 years and increases the variability of the model climate between major cycles, but has only a small effect on shape or period of the large-magnitude cycles.

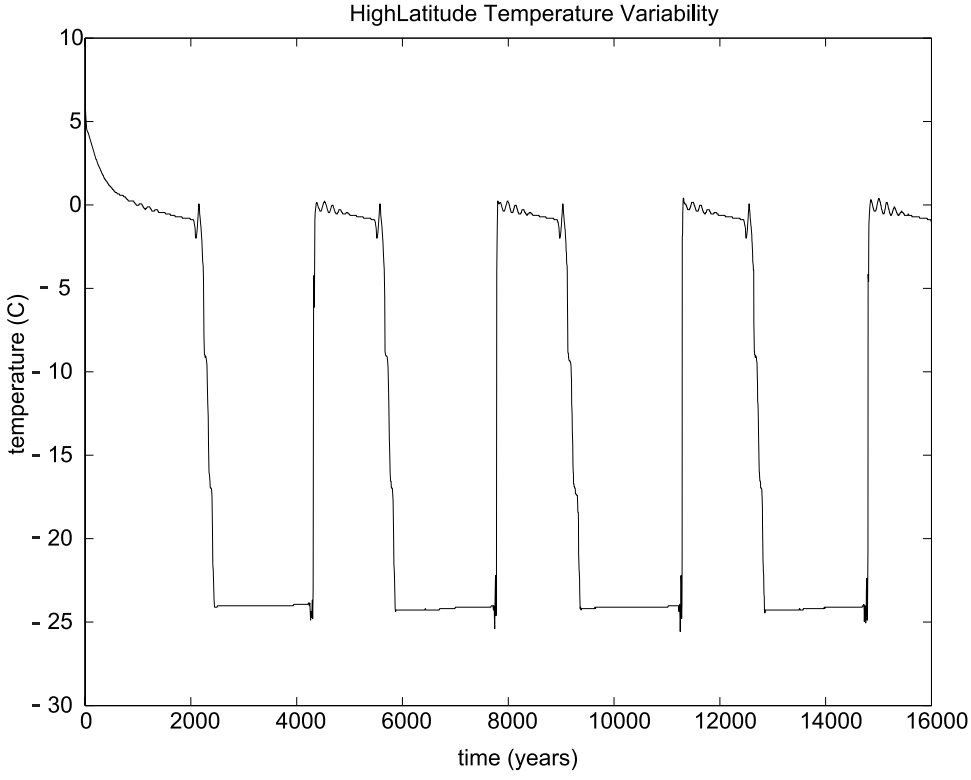

Figure 13. Time series of atmospheric temperature in the e = 0.73 experiments without stochastic forcing. There is less variability in the amplitude and period of the temperature oscillations when no stochastic forcing is applied compared to oscillations with stochastic forcing.

[77] Finally, let us mention a main limitation of this work, namely the use of a single-hemisphere ocean basin. This cannot correctly represent the geography of the North Atlantic Ocean and so features such as exact latitude or depth of a particular event cannot be credibly compared to the geologic record. This of itself is of little consequence, but perhaps more seriously, interhemispheric phenomena cannot be modeled, and so one might argue the model is seriously deficient. However, we may invert such reasoning, and argue that the ability of the simple model to produce reasonably realistic circulation has allowed the essential mechanism to be extracted more easily, and further suggests that interhemispheric variations, while certainly present in the historical record, are a consequence and not a cause of a mechanism that has its roots in the North Atlantic. A related issue is that in some theoretical and numerical models of the overturning circulation, an important role is played by the wind forcing in the Antarctic Circumpolar Current [*Toggweiler and Samuels*, 1998; *Vallis*, 2000]. However, in addition to that wind, the presence of a source of dense water in the North Atlantic is necessary to produce such a circulation, and sea ice cover in the North Atlantic will certainly affect this. In that case, of course, the value of the diffusivity would play a lesser role. Clearly, the next step is to use a more realistic model that allows interhemispheric and even interbasin exchanges, for these are important aspects of the real climate system.

[78] In summary, our results support the notion that the overturning circulation of the ocean plays a significant role in the variability of glacial climates. More specifically, we suggest that cooling and the growth of sea ice and the corresponding weakness and instability of the overturning circulation are responsible for this variability, and we have offered a mechanism whereby this may occur. The mechanism is sufficient to explain the presence and some of the properties of Dansgaard-Oeschger cycles during glacial cycles and the relative stability of the Holocene.

Appendix A

[79] The equations for the four-box model are

Ocean salinity equations:

$$\frac{dS_l}{dt} = \frac{3M_{ld}}{hL}(S_d - S_l) + \frac{3M_{lm}}{hL}(S_h - S_l) + \frac{F_s}{h} \tag{A1}$$

$$\frac{dS_h}{dt} = \frac{3M_{hd}}{hL}(S_d - S_h) + \frac{3M_{hm}}{hL}(S_l - S_h) - \frac{F_s}{h} \tag{A2}$$

$$\frac{dS_m}{dt} = \frac{3M_{md}}{hL}(S_d - S_m) + \frac{3M_{lm}}{hL}[(S_l - S_m) + (S_h - S_m)] \tag{A3}$$

$$\frac{dS_d}{dt} = \frac{M_{ld}}{HL}(S_l - S_d) + \frac{M_{hd}}{HL}(S_h - S_d) + \frac{M_{md}}{HL}(S_m - S_d) \tag{A4}$$

Table A1. Constants for Four-Box Model and for Linear Equation of State[a]

Symbol	Description	Value
L	length scale	6.37×10^6 m
H	deep ocean length scale	500 m
h	mixed layer depth	50 m
$H(L/2)M_{ld}$	low-latitude surface/deep heat transport	200 years
$H(L/2)M_{hd}$	high-latitude surface/deep heat transport	200 years
$H(L/2)M_{lh}$	surface heat/salinity transport	5 years
$1/\lambda_{ao}$	atmosphere to ocean heat transport	0.89 years
$1/\lambda_{oa}$	ocean to atmosphere heat transport	0.045 years
$1/\mu$	latitudinal atmosphere heat transport	0.08 years
$1/\gamma$	atmosphere restoring time	0.074 years
α	fractional ice cover	no ice 0 – maximum ice 1
F_s	salinity flux	$(35\ \text{kg m}^{-3})*(0.55\ \text{m yr}^{-1})$
ρ_0	reference density	1026.95 kg m^{-3}
T_0	reference temperature	283 K
S_0	reference salinity	35
β_s	haline contraction coefficient	0.78×10^{-3}
β_l	linear thermal expansion coefficient	9.0×10^{-5}

[a]Sources are *Winton* [1993] and *Rahmstorf* [1994].

Ocean temperature equations:

$$\frac{dT_l}{dt} = \frac{3M_{ld}}{hL}(T_d - T_l) + \frac{3M_{lm}}{hL}(T_h - T_l) + \lambda_{ao}(T_{al} - T_l) \tag{A5}$$

$$\frac{dT_h}{dt} = \frac{3M_{hd}}{hL}(T_d - T_h) + \frac{3M_{lm}}{hL}(T_l - T_h) + (1 - \alpha_h)\lambda_{ao}(T_{ah} - T_h) + \alpha_h\lambda_{ao}(271.0 - T_h) \tag{A6}$$

$$\frac{dT_m}{dt} = \frac{3M_{md}}{hL}(T_d - T_m) + \frac{3M_{lh}}{hL}[(T_l - T_m) + (T_h - T_m)] \tag{A7}$$

$$\frac{dT_d}{dt} = \frac{M_{ld}}{HL}(T_l - T_d) + \frac{M_{hd}}{HL}(T_h - T_d) + \frac{M_{md}}{HL}(T_m - T_d) \tag{A8}$$

Atmosphere equations:

$$\frac{dT_{ah}}{dt} = (1 - \alpha_h)\lambda_{oa}(T_h - T_{ah}) - \alpha_h\lambda_{oa}(271.0 - T_h) + \mu(T_{am} - T_{ah}) + \gamma(T_{hres} - T_{ah}) \tag{A9}$$

$$\frac{dT_{al}}{dt} = \lambda_{oa}(T_l - T_{al}) + \mu(T_{al} - T_{am}) + \gamma(T_{lres} - T_{al}) \tag{A10}$$

$$T_{am} = \frac{T_{al} + T_{ah}}{2} \tag{A11}$$

Equation of state:

$$\rho = \rho_0[1 - \beta_l(T - T_0) + \beta_S(S - S_0)] \tag{A12}$$

[80] T_{hres} and T_{lres} are atmosphere restoring temperatures. The equations for the high- and low-latitude atmosphere temperature (T_{ah}, T_{am}) are solved for the steady state condition where $dT_{ah}/dt = 0.0$ and $dT_{al}/dt = 0.0$. The fractional ice cover (α) varies linearly with the associated atmosphere temperature. When the atmosphere temperature (T_{ah}, T_{am}) is 271 K or above there is no ice ($\alpha = 0$), and when the atmosphere temperature is 261 K or below, the associated box becomes completely covered with ice ($\alpha = 1.0$). Additional constants used in this model are taken from *Winton* [1993] and *Rahmstorf* [1994] and are summarized in Table A1.

[81] To provide for convective adjustment, when the water column becomes unstable, ($\rho(T_{\{l,h\}}, S_{\{l,h\}}) > \rho(T_d, S_d)$), M_{ld}, M_{hd} and M_{md} are multiplied by 10 [*Winton*, 1995].

References

Alley, R. B., S. Anandakrishnan, and P. Jung (2001), Stochastic resonance in the North Atlantic, *Paleoceanography*, *16*(2), 190–198.

Bender, M., T. Sowers, M. L. Dickson, J. Orchardo, P. Grootes, P. A. Mayewski, and D. A. Meese (1994), Climate correlations between Greenland and Antarctica during the past 100,000 years, *Nature*, *327*, 663–666.

Bianchi, G. G., and I. N. McCave (1999), Holocene periodicity in North Atlantic climate and deep ocean flow south of Iceland, *Nature*, *397*, 515–517.

Bigg, G., D. Wadley, D. Stevens, and J. Johnson (2000), Glacial thermohaline circulation states of the North Atlantic: The compatibility of modeling and observations, *J. Geol. Soc. London*, *157*, 655–665.

Blunier, T., et al. (1999), Warming of the tropical Atlantic Ocean and slowdown of the thermo-

haline circulation during the last deglaciation, *Nature*, *402*, 511–514.
Bond, G., W. Broecker, S. Johnsen, J. McManus, L. Labeyrie, J. Jouzel, and G. Bonani (1993), Correlations between climate records from North Atlantic sediment and Greenland ice, *Nature*, *365*, 143–147.
Bond, G., et al. (1997), A pervasive millennial-scale cycle in North Atlantic Holocene and glacial climates, *Science*, *278*, 1257–1266.
Boyle, E. A., and L. D. Keigwin (1985), Comparison of Atlantic and Pacific paleochemical records for the last 215,000 years: Changes in deep ocean circulation and chemical inventories, *Earth Planet. Sci. Lett.*, *76*, 135–150.
Boyle, E. A., and L. D. Keigwin (1987), North Atlantic thermohaline circulation during the past 20,000 years linked to high-latitude surface temperature, *Nature*, *330*, 35–40.
Broecker, W. S. (1996), Glacial climate in the tropics, *Science*, *272*, 1902–1904.
Broecker, W. S., and S. Hemming (2001), Climate swings come into focus, *Science*, *294*, 2308–2309.
Broecker, W. S., G. Bond, M. Klas, G. Bonani, and W. Wolfli (1990), A salt oscillator in the glacial Atlantic?, *Paleoceanography*, *5*(4), 469–477.
Bryan, F. (1986), High-latitude salinity effects and the interhemispheric thermohaline circulations, *Nature*, *323*, 301–304.
Clark, P. U., N. G. Pisias, T. F. Stocker, and A. J. Weaver (2002), The role of the thermohaline circulation in abrupt climate change, *Nature*, *415*, 863–869.
CLIMAP Project Members (1976), The surface of the ice-age Earth, *Science*, *191*, 1131–1138.
Dansgaard, W., S. J. Johnsen, H. B. Clausen, D. Dahl-Jensen, A. N. Gundestrup, and C. U. Hammer (1984), North Atlantic climactic oscillations revealed by deep Greenland ice cores, in *Climate Processes and Climate Sensitivity*, *Geophys. Monogr. Ser.*, vol. 29, edited by J. E. Hanson and T. Takahashi, pp. 288–298, AGU, Washington, D. C.
Dansgaard, W., et al. (1993), Evidence for general instability of past climate from a 250-kyr ice-core record, *Nature*, *364*, 218–220.
de Vernal, A., and C. Hillaire-Marcel (2000), Sea-ice cover, sea-surface salinity and halo-/themocline structure of the northwest North Atlantic: Modern versus full glacial conditions, *Quat. Sci. Rev.*, *19*, 65–85.
de Vernal, A., C. Hillaire-Marcel, J.-L. Turon, and J. Matthiessen (2000), Reconstruction of sea-surface temperature, salinity and sea ice cover in the northern North Atlantic during the Last Glacial Maximum based on dinocyst assemblages, *Can. J. Earth Sci.*, *37*, 725–750.
Duplessy, J. C., N. J. Shackleton, R. G. Fairbanks, L. Labeyrie, D. W. Oppo, and N. Kallel (1988), Deep water source variations during the last climatic cycle and their impact on the global deep water circulation, *Paleoceanography*, *3*(3), 343–360.
Duplessy, J. C., L. Labeyrie, A. Juillet-LeClerc, F. Naitre, J. Duprat, and M. Sarnthein (1991), Surface salinity reconstruction of the North Atlantic Ocean during the Last Glacial Maximum, *Oceanol. Acta*, *14*, 311–324.
Fanning, A. F., and A. J. Weaver (1996), An atmospheric energy-moisture balance model: Climatology, interpentadal climate change, and coupling to an ocean general circulation model, *J. Geophys. Res.*, *101*, 15,111–15,128.
Ganachaud, A., and C. Wunsch (2000), Improved estimates of global ocean circulation, heat transport and mixing from hydrographic data, *Nature*, *408*, 453–457.
Ganopolski, A., and S. Rahmstorf (2001), Rapid changes of the glacial climate simulated in a coupled climate model, *Nature*, *409*, 153–158.
Gildor, H., and E. Tziperman (2000), Sea ice as the glacial cycles' climate switch: Role of seasonal and orbital forcing, *Paleoceanography*, *15*(6), 605–615.
Gildor, H., and E. Tziperman (2003), Sea-ice switches and abrupt climate change, *Philos. Trans. R. Soc. London, Ser. A*, *361*, 1935–1944.
Heinrich, M. (1988), Origin and consequences of cyclic ice rafting in the northeast Atlantic Ocean during the past 130,000 years, *Quat. Res.*, *2*, 143–152.
Johnsen, S. J., H. B. Clausen, W. Dansgaard, K. Fuhrer, N. Gunderstrup, C. U. Hamjmer, P. Iversen, J. Jousel, B. Stauffer, and J. P. Steffensen (1992), Irregular glacial interstadials recorded in a new Greenland ice core, *Nature*, *359*, 311–313.
Jouzel, J., et al. (1993), Extending the Vostock ice-core record of paleoclimate to the penultimate glacial period, *Nature*, *364*, 407–412.
Kaspi, Y., R. Sayag, and E. Tziperman (2004), A "triple sea-ice state" mechanism for the abrupt warming and synchronous ice sheet collapses during Heinrich events, *Paleoceanography*, *19*, PA3004, doi:10.1029/2004PA001009.
Keigwin, L. D., and G. A. Jones (1994), Western North Atlantic evidence for millennial-scale changes in ocean circulation and climate, *J. Geophys. Res.*, *99*, 12,397–12,410.
Keigwin, L. D., and S. J. Lehman (1994), Deep circulation change linked to Heinrich event 1 and the Younger Dyras in a midepth North Atlantic core, *Paleoceanography*, *9*(2), 185–194.
Keigwin, L. D., W. B. Curry, S. J. Lehman, and S. Johnsen (1994), The role of the deep ocean in North Atlantic climate change between 70 and 130 kyr ago, *Nature*, *371*, 323–325.
Lohmann, G., and R. Gerdes (1998), Sea ice effects on the sensitivity of the thermohaline circulation, *J. Clim.*, *11*, 2789–2803.
MacAyeal, D. (1993), Binge/purge oscillations of the Laurentide ice sheet as a cause of the North Atlantic's Heinrich events, *Paleoceanography*, *8*, 775–784.
Manabe, S., and R. J. Stouffer (1988), Two stable equilibria of a coupled ocean-atmosphere model, *J. Clim.*, *1*, 841–866.
Manabe, S., and R. J. Stouffer (1995), Simulation of abrupt climate change induced by freshwater input to the North Atlantic Ocean, *Nature*, *378*, 165–167.
Manabe, S., and R. J. Stouffer (1997), Coupled ocean-atmosphere model response to freshwater input: Comparison to Younger Dryas event, *Paleoceanography*, *12*(2), 321–336.
Oppo, D. W., and S. J. Lehman (1993), Mid-depth circulation of the subpolar North Atlantic during the Last Glacial Maximum, *Science*, *259*, 1148–1152.
Oppo, D. W., and S. J. Lehman (1995), Suborbital timescale variability of the North Atlantic Deep Water during the past 200,000 years, *Nature*, *10*, 901–910.
Parkinson, C. L., and W. M. Washington (1979), A large-scale numerical model of sea ice, *J. Geophys. Res.*, *84*, 311–337.
Pflaumann, U., et al. (2003), Glacial North Atlantic: Sea-surface conditions reconstructed by GLAMAP 2000, *Paleoceanography*, *18*(3), 1065, doi:10.1029/2002PA000774.
Rahmstorf, S. (1994), Rapid climate transitions in a coupled ocean-atmosphere model, *Nature*, *372*, 82–85.
Rahmstorf, S. (2002), Ocean circulation and the climate during the past 120,000 years, *Nature*, *419*, 207–214.
Rahmstorf, S. (2003), Thermohaline circulation: The current climate, *Nature*, *421*, 699.
Ruhlemann, C., S. Mulitza, P. J. Muller, W. Gerold, and R. Zahn (1999), Warming of the tropical Atlantic Ocean and slowdown of the thermohaline circulation during the last deglaciation, *Nature*, *402*, 511–514.
Rutberg, R. L., S. R. Hemming, and S. L. Goldstein (2000), Reduced North Atlantic Deep Water flux to the glacial Southern Ocean inferred from neodymium isotope ratios, *Nature*, *405*, 935–938.
Sakai, K., and W. R. Peltier (1997), Dansgaard-Oeschger oscillations in a coupled atmosphere-ocean climate model, *J. Clim.*, *10*, 949–970.
Sakai, K., and W. R. Peltier (1999), A dynamical systems model of the Dansgaard-Oeschger oscillation and the origin of the Bond cycle, *J. Clim.*, *12*, 2238–2255.
Samelson, R. M., and G. K. Vallis (1996), A simple friction and diffusion scheme for planetary-geostrophic basin models, *J. Phys. Oceanogr.*, *27*, 186–194.
Samelson, R. M., and G. K. Vallis (1997), Large-scale circulation with small diapycnal diffusion: The two thermocline limit, *J. Mar. Res.*, *55*, 223–275.
Sarnthein, M., et al. (1995), Variations in Atlantic surface ocean paleoceanography 50°–80°N: A time-slice record of the last 30,000 years, *Paleoceanography*, *10*(6), 1063–1094.
Semtner, A. J. (1976), A model for thermodynamic growth of sea ice in numerical investigations of climate, *J. Phys. Oceanogr.*, *6*, 379–389.
Severinghaus, J. P., T. Sowers, E. J. Brook, R. B. Alley, and M. L. Bender (1998), Timing of abrupt climate change at the end of the Younger Dryas interval from thermally fractionated gases in polar ice, *Nature*, *391*, 141–146.
Stocker, T. F., and D. G. Wright (1991), Rapid transitions of the ocean's deep circulation induced by changes in surface water fluxes, *Nature*, *351*, 729–732.
Stommel, H. (1961), Thermohaline convection with two stable regimes of flow, *Tellus*, *13*, 224–230.
Taylor, K. C., G. W. Lamoray, G. A. Doyle, R. B. Alley, P. M. Grootes, P. A. Mayewski, W. C. White, and L. Barlow (1993), The "flickering switch" of late Pleistocene climate change, *Nature*, *361*, 432–435.
Toggweiler, J. R., and B. Samuels (1998), On the ocean's large-scale circulation in the limit of no vertical mixing, *J. Phys. Oceanogr.*, *28*, 1832–1852.
Tziperman, E. (1997), Inherently unstable climate behaviour due to weak thermohaline ocean circulation, *Nature*, *386*, 592–595.

Vallis, G. K. (2000), Large-scale circulation and production of stratification: Effects of wind, geometry and diffusion, *J. Phys. Oceanogr.*, *30*, 933–954.

Voelker, A. H. L. (2002), Global distribution of centennial scale records for marine isotope stage 3: A database, *Quat. Sci. Rev.*, *21*, 1185–1214.

Weaver, A. J., E. S. Sarachik, and J. Marotzke (1991), Freshwater flux forcing during decadal and interdecadal oceanic variability, *Nature*, *353*, 836–838.

Winton, M. (1993), Deep decoupling oscillations of the oceanic themohaline circulation, in *Ice in the Climate System*, *NATO ASI Ser., Ser I*, vol. 12, edited by W. R. Peltier, pp. 417–432, Springer, New York.

Winton, M. (1995), The effect of cold climate upon North Atlantic Deep Water formation in a simple ocean-atmosphere model, *J. Clim.*, *10*, 37–51.

J. L. Loving, Department of Ocean Sciences, University of California, Santa Cruz, Santa Cruz, CA 95064, USA.

G. K. Vallis, GFDL, Princeton University, Princeton, NJ 08544, USA. (gkv@princeton.edu)

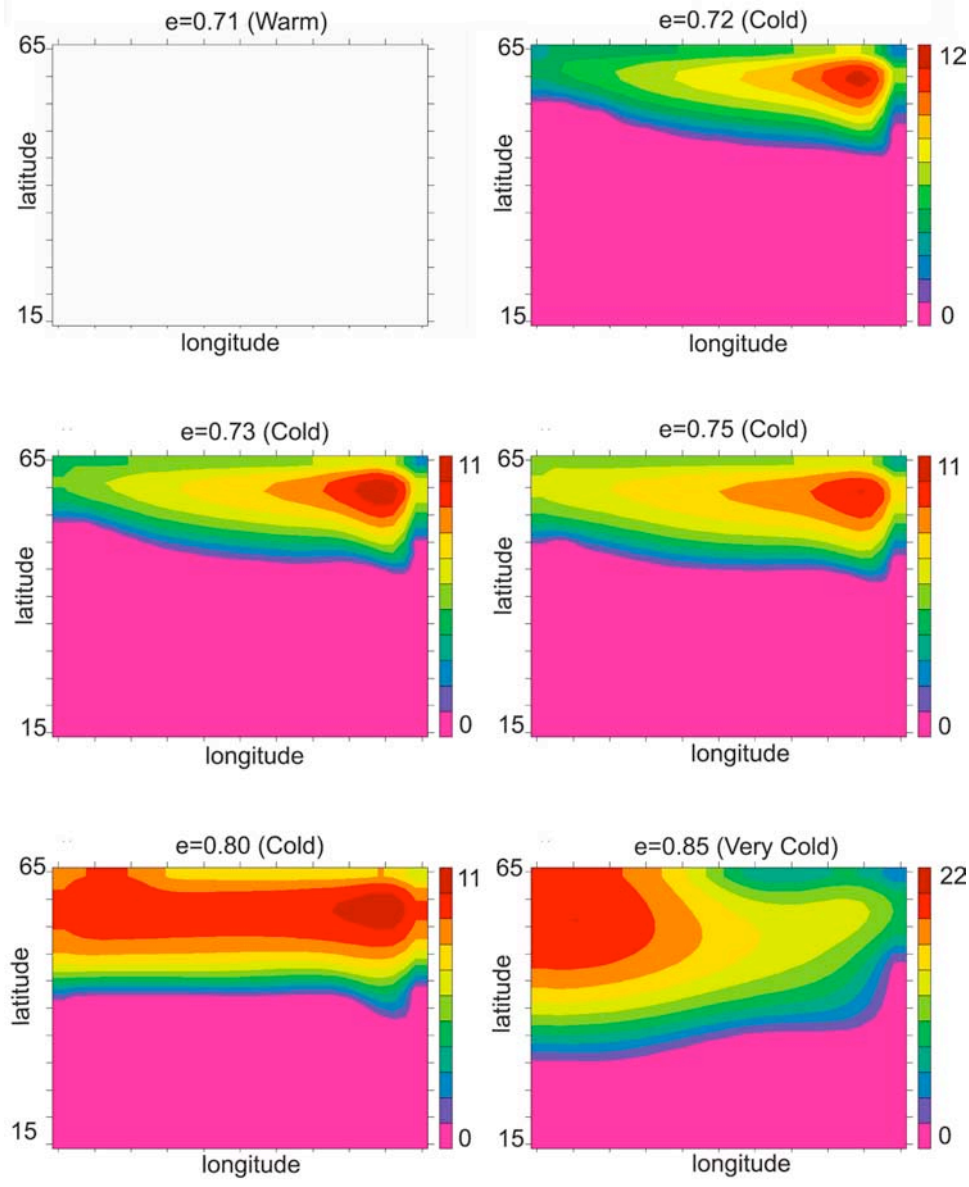

Figure 3. Sea ice thickness and extent for "cooling without freshening" experiments. In the warmest experiment (e = 0.71), there is no sea ice. In the cold experiments (e = 0.72 to 0.85), sea ice forms and expands. In the coldest experiment (e = 0.85), sea ice covers almost half of the basin. The region of constant temperature, near-freezing, surface water expands with the sea ice edge (not shown).

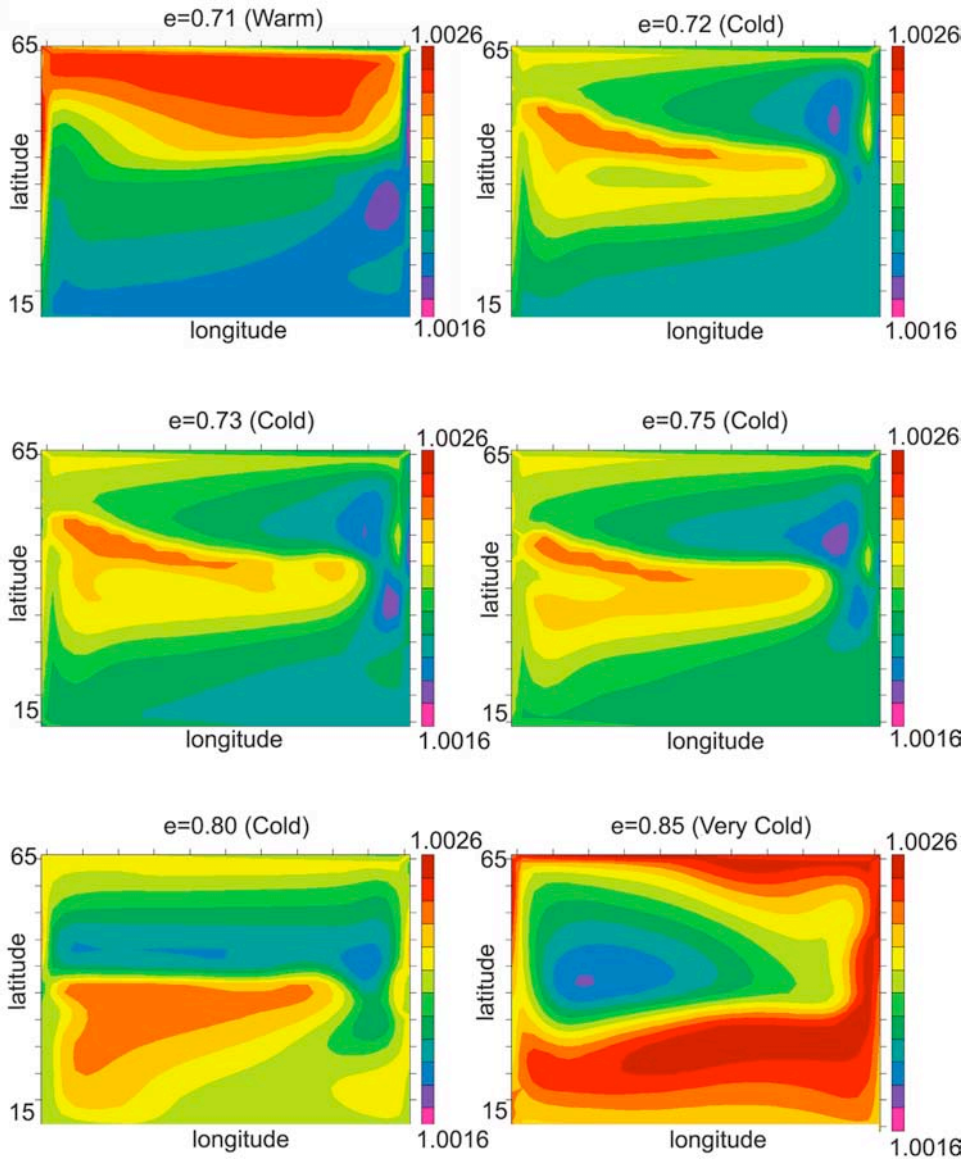

Figure 4. Surface density for "cooling without freshening" experiments. In the warmest experiment (e = 071) the highest density water is along the northern boundary where deep water is forming. In the cold experiments (e = 0.72 to 0.80) the sinking region shifts southward. In the coldest experiment (e = 0.85) the highest-density water is along the southern boundary, and there is weak reverse overturning.

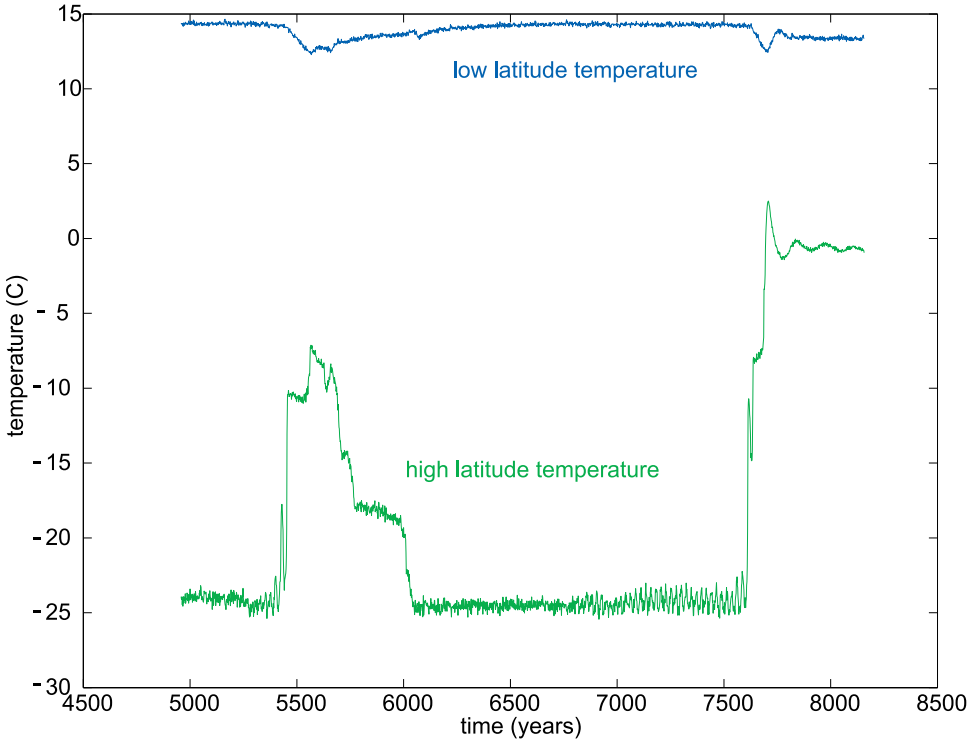

Figure 6. Atmosphere-temperature time series for two warm events in the e = 0.73 "cooling without freshening" experiment. The high-latitude atmosphere temperature change is out of phase with the low-latitude temperature change. The low-latitude temperature change is gradual, and the temperature change at high latitudes is more abrupt and higher amplitude. The small-amplitude warm event displays the distinct sawtooth profile for the high-latitude atmosphere temperature.

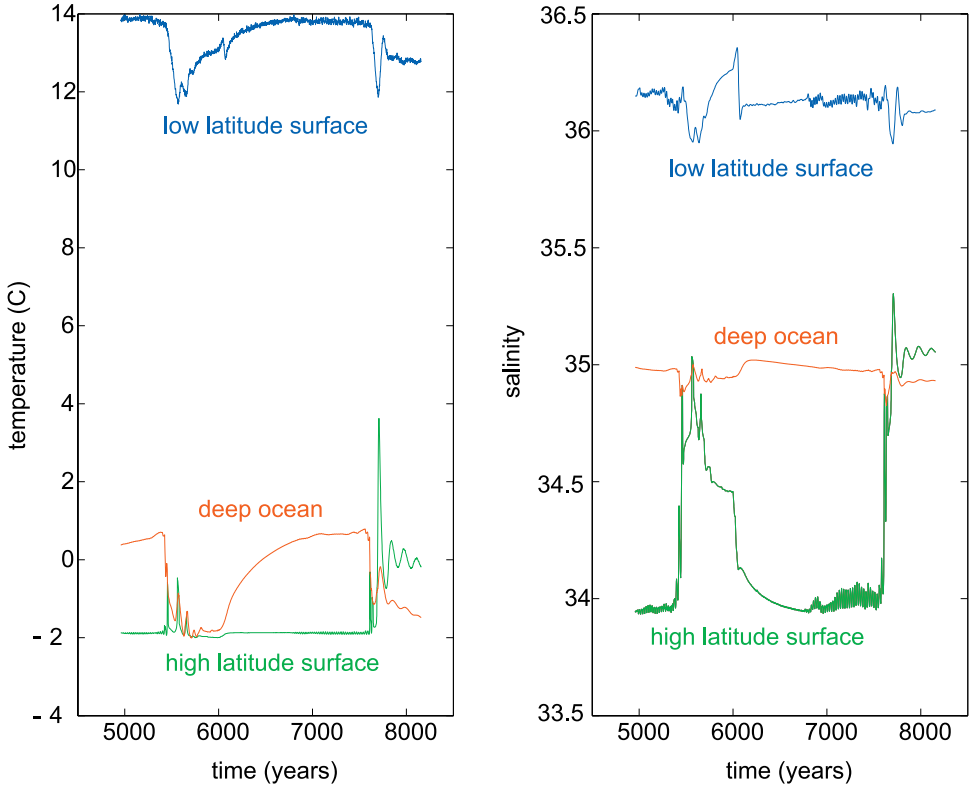

Figure 7. Time series of high-latitude, low-latitude and deep ocean temperature and salinity for the e = 0.73 experiment. (left) The high-latitude sea surface temperature changes by a few degrees over a single oscillation. At low latitudes and in the deep ocean, sea surface temperature changes are smaller. During warm events the (right) high-latitude salinity increases abruptly while the deep ocean and low-latitude surface salinity decreases.

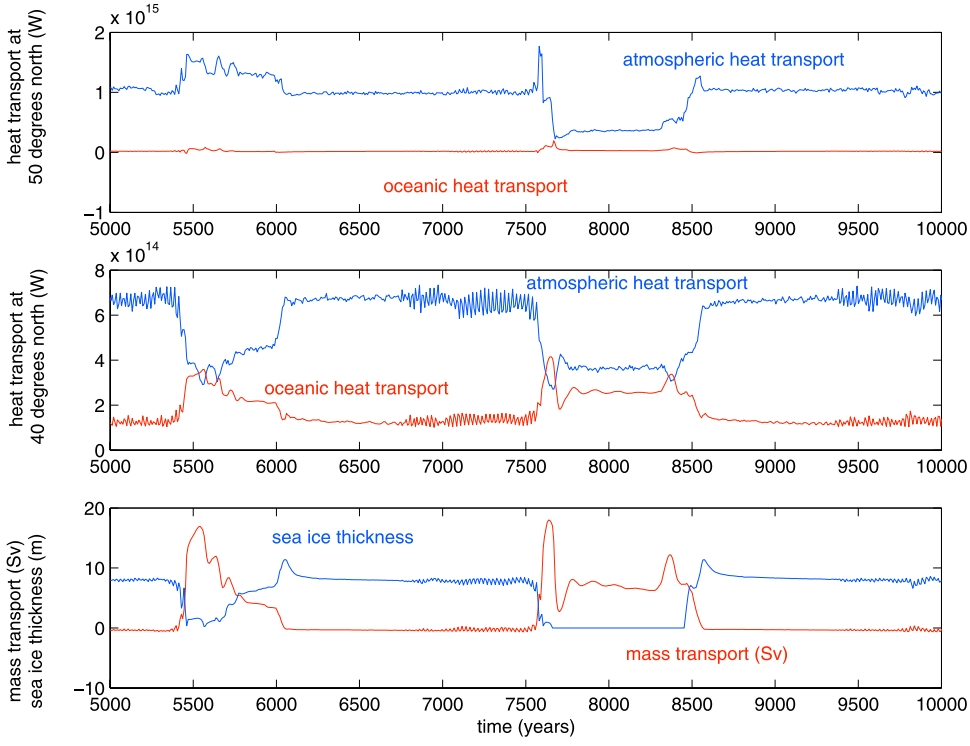

Figure 8. Time series of oceanic (red) and atmospheric (blue) meridional heat transport at (top) 50°N and (center) 40°N. (bottom) Maximum overturning circulation in sverdrups (red) and sea ice thickness (blue). The oceanic heat transport (red) increases over both warming cycles at 40°N, and the atmospheric heat transport (blue) decreases. (top) The increase in meridional heat transport by the ocean is accompanied by (bottom) an increase in mass transport by the ocean. The reduction in heat transport by the atmosphere is associated with a reduction in the atmospheric temperature gradient (Figure 6). The (top) 50°N location is near the sea ice edge where the meridional temperature gradient in the atmosphere is very large.

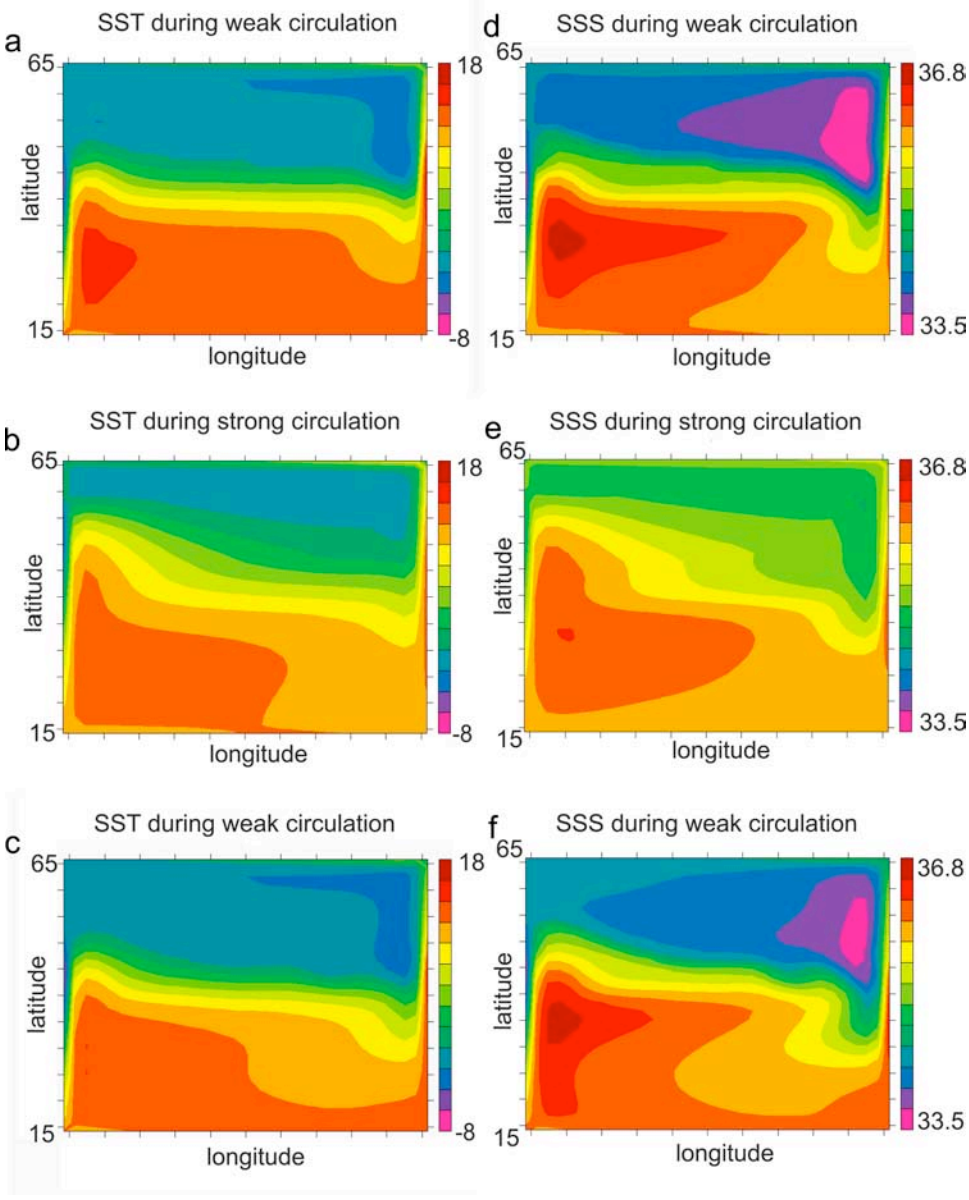

Figure 10. Sea surface temperature and salinity at various times over one cycle for the e = 0.73 experiment. (a) SST at the weakest point in the circulation. The cold region in the north extends to about the middle of the basin. (b) SST for a strong circulation. Note the northern ocean warms and the southern ocean cools. (c) SST with the circulation in its weak phase again. (d–f) Sea surface salinity during periods corresponding to Figures 10a–10c. During weak periods in the circulation (Figures 10d and 10f) the high-latitude sea surface freshens.

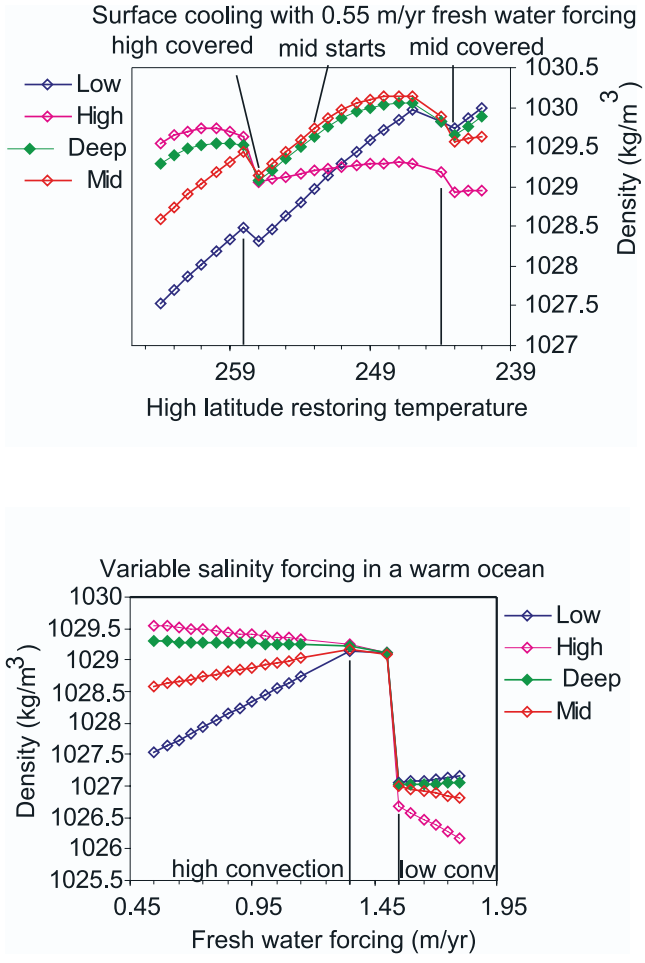

Figure 12. Four box model results. (top) Density against high-latitude restoring temperature for each box in the "cooling without freshening" experiments. In these experiments the circulation transitions from high-latitude convection to midlatitude convection and finally to low-latitude convection. (bottom) Density for each box in experiments where we increased the high-latitude freshwater forcing in a warm climate. The shift to midlatitude convection does not occur in these warm climate results, and the circulation shifts directly from high- to low-latitude sinking when sufficient freshwater forcing is applied.